Copyright © 1966, by the author(s).
All rights reserved.

Permission to make digital or hard copies of all or part of this work for personal or classroom use is granted without fee provided that copies are not made or distributed for profit or commercial advantage and that copies bear this notice and the full citation on the first page. To copy otherwise, to republish, to post on servers or to redistribute to lists, requires prior specific permission.

CONTRAST FORMATION IN THE SCANNING ELECTRON MICROSCOPE

by

T. E. Everhart

Memorandum ERL-M161

26 August 1966

ELECTRONICS RESEARCH LABORATORY

College of Engineering
University of California, Berkeley
94720

Manuscript submitted: 2 May 1966

The research reported herein was supported wholly by the Air Force Avionics Laboratory, Research and Technology Division, Wright-Patterson Air Force Base, Ohio, under Contract No. AF33(615)-2306.

CHAPTER 1.

INTRODUCTION

1.1. A Brief Historical Perspective.

For many centuries the smallest object which man could see was determined by the resolution of the human eye. Although simple magnifying glasses were known before the birth of Christ, the compound microscope was not invented until about 1590, and highly corrected microscope lenses were not developed until late in the last century, when a wide variety of optical glasses became available. Although the compound light microscope is and will continue to be a valuable research tool, it suffers from two fundamental limitations: (1) its maximum resolution is limited by diffraction to between 1000 and 2000 A. (A. = Angstrom unit = 10^{-8} cm.), and (2) it has a very limited depth of field.

Following de Broglio's theory of the wave nature of matter in 1925, and the development of electron optics, scientists saw that much higher resolutions could be attained with an electron microscope. If the limit set by diffraction alone could be reached, the maximum resolution would be ≤ 0.1 A. for electron energies ≥ 15 kv. In

practice electron lens aberrations have limited the maximum resolution to about 5 A., which is 200 to 400 times better than that obtained with the light microscope. Because the electron microscope must use small apertures to minimize lens aberrations, electron micrographs show a much greater depth of field than light micrographs. These fundamental advantages have greatly stimulated the development of the electron microscope; in little more than twenty-five years it has been transformed from an idea into a practical research tool which is finding ever increasing applications.

The conventional or transmission electron microscope has been discussed thoroughly by several authors (Zworykin et al, (1945), Cosslett (1951), Hall (1953), for example) and its general capabilities may be taken as common knowledge. This instrument is limited to examining thin films from about 50 to 500 A. thick. The continuous development of replica techniques has greatly expanded the potentialities of the transmission instrument, until today it is used more widely than any other type of electron microscope. Other instruments presently used for certain applications are the reflection microscope, the mirror microscope, the field and ion emission microscopes, and the scanning microscope. The closely related X-ray instruments, the reflection X-ray microscope, the projection X-ray microscope, the X-ray micro-analyser, and the scanning X-ray microscope should also be mentioned. This list is not meant

to be exhaustive, and for a comprehensive discussion and comparison of these instruments, the reader is referred to Smith (1956).

The scanning microscope, which is the subject of this dissertation, is one of these instruments which complement the conventional transmission electron microscope. Opaque surfaces can be observed directly in the scanning microscope, obviating replication. Kinetic processes, such as chemical decomposition, can be watched in it, and the possibility of observing living organisms also exists (Smith, 1956, Sections 10.3 and 9.5).

The scanning electron microscope was first proposed by Knoll in 1935; three years later a transmission scanning microscope was described by von Ardenne (1938), and in 1942 Zworykin, Hillier, and Snyder (1942) reported that an instrument designed primarily to study opaque surfaces had been constructed. An improved scanning microscope has more recently been built at Cambridge by McMullan (1952, 53); its main advantages were a simplified column, the first directly viewed image, and a better signal-to-noise ratio. Smith (1956) improved this instrument, obtaining a resolution of about 250 A., and also surveyed several fields of application. Wells (1957) constructed a "Mark II" model of this instrument, and used it to study fibres.

1.2. Principles of Scanning Electron Microscopy.

The scanning electron microscope may be described as a closed circuit television system. An electron beam is focused to a very small diameter spot or probe which is then scanned in a raster pattern over the specimen surface. A cathode-ray tube (CRT) is scanned simultaneously in an identical raster pattern, and therefore a one-to-one correspondence exists between any point on the scanned area of the specimen and the corresponding point on the scanned area of the CRT screen. If the specimen is scanned in a square raster of side s, and the CRT is scanned in a similar raster of side S, the instrumental magnification M is S/s. If the maximum resolution of the scanned area of the CRT screen is L lines, the maximum number of picture elements in the image is limited to L^2. At all but the highest magnifications the resolution of the instrument is $S/LM = s/L$; the maximum resolution is set by the diameter of the electron probe, which is about 250 A. in the present instrument.

In the usual mode of operation, the normal to the specimen surface and the axis of the primary beam meet in roughly a 60° angle. In this configuration the secondary electron current produced by the primary beam varies with the specimen geometry; when this current is collected and amplified, and the resulting video signal modulates the CRT brightness, an image related to specimen geometry is formed on the CRT screen. The permanent record obtained by

photographing this image is called a reflection scanning electron micrograph, or more simply, a micrograph.

If the primary beam is perpendicular to the specimen surface, and the specimen is thin so most primary electrons penetrate it and are collected, the image brightness is a measure of the specimen opacity to the primary beam. This mode of operation is useful for alignment, and certain special applications; the record in this case is a transmission scanning electron micrograph, or more simply, a transmission micrograph.

1.3. The Author's Research.

When the author's research began in October 1955, contrast formation in the scanning microscope was not understood. McMullan (1952, Chapter 8) explained contrast formation when the video signal is due only to reflected electrons, i.e., those electrons coming from the bombarded specimen with energies between 50 ev. and the primary beam energy of many kev. Using a different collection geometry, Smith (1956, p. 125) subsequently surmised that most of the video signal was due to secondary electrons, (those electrons coming from the bombarded specimen with energies less than 50 ev.). Since intelligent scanning electron microscope design and the correct interpretation of micrographs require an understanding of contrast formation, this understanding became the author's primary objective.

Secondary objectives were new applications of the instrument, such as the microscopic study of potential boundaries on specimen surfaces, and instrumental improvements, often necessary because of equipment failure, or because the existing instrument was not suited to the planned research.

Contrast is intimately connected with the secondary and reflected electrons, defined above. The ratios of the secondary electron current and the reflected electron current to the primary beam current will be called the secondary electron coefficient, δ_s, and the reflection coefficient, r. The total current coming from the specimen will be called the secondary emission; the ratio of this current to the primary beam current is commonly called either the secondary emission coefficient or the secondary yield, and is denoted by δ. It follows that

$$\delta = \delta_s + r. \tag{1}$$

Before further discussion of the primary objective, contrast formation, the term contrast will be defined. Usually the contrast of a picture element is related to the brightness of that element, B, and the background brightness of the picture, B_o, by the definition,

$$C = \frac{B - B_o}{B_o} \tag{2}$$

(see for example Zworykin and Morton (1954) p. 179).

When examining an electron micrograph, where the resolution of neighbouring picture elements of brightness B_1 and B_2 is most important, the contrast between these elements in terms of this definition is

$$C_{12} = C_2 - C_1 = \frac{B_2 - B_1}{B_o} . \tag{3}$$

The background brightness, not a well defined quantity, is still present in this equation. To eliminate B_o, contrast will be defined in this thesis as the difference in brightness between two picture elements, divided by the brightness of the brighter element,

$$C = \frac{B - B_1}{B} = \Delta B/B, \qquad B \geq B_1. \tag{4}$$

By this definition $0 \leq C \leq 1$. This definition will facilitate the discussion of contrast in terms of the number of electrons per picture element, and will prove particularly useful when contrast expansion and noise are discussed.

The contrast observed on a scanning electron micrograph depends on (1) the primary beam current incident on each picture element of the specimen surface, (2) the specimen itself, (3) the collection system, and (4) the display and recording system. The cathode temperature, the primary electron energy, the electron-

optical system, and the rate of scan of the primary beam over the specimen surface are factors which determine the number of electrons incident on each picture element of the specimen surface. The specimen's thickness, its geometry, density, conductivity, and potential may all influence contrast, as may any contaminating layers which form upon it. The geometry of the collector system (which influences the collection efficiency), the collector voltage, and the collector sensitivity to electrons of different energies are also important considerations. Finally, the gamma of the display and recording system, the black level setting, and the video signal amplitude also influence contrast.

Earlier treatments of the fundamental limitations of the scanning electron microscope have neglected the noise introduced by secondary emission at the specimen; including this noise leads to a more pessimistic answer for the theoretical maximum resolution of the scanning electron microscope at a given contrast and recording time. A simple theory concerning reflected electrons is presented, which successfully explains much of the observed data. This theory leads to a more complete understanding of the various phenomena taking place as the primary beam strikes the specimen, and also leads to a self-consistent explanation of certain aspects of secondary emission,

including noise and the depth of origin of secondary electrons, both important when considering the maximum resolution of the scanning electron microscope.

A discussion of all these subjects is presented in the following chapters. Choosing the order in which interrelated parts of a complex topic are presented is a perplexing problem; the order followed in this thesis was chosen to minimize the use of the phrase: "It will be shown later....". Where the order was not obvious on this basis, a roughly chronological order was chosen.

CHAPTER 2.

THE COLLECTION SYSTEM

The collection system must collect a large fraction of the electrons emerging from the specimen, and amplify them into a current large enough to be handled by ordinary valve amplifiers. A system designed to collect reflected electrons may differ significantly from one designed to collect secondary electrons, for according to Sternglass (1954), the mean energy of the reflected electrons is about half the primary energy, i.e., several thousand electron volts, while the mean energy of the secondary electrons is only a few electron volts. Both McMullan and Smith designed their collection systems for reflected electrons; that a significant proportion of the secondary electrons were collected and amplified by Smith's system is a fortuitous consequence of the original choice of a positively biased electron multiplier as the electron collector and preamplifier. If an unbiased scintillator had been chosen instead, the secondary electrons would not have been recorded, and might have gone completely unnoticed.

2.1. The Electron Multiplier Collection System.

Smith's electron multiplier collector arrangement is drawn

to scale in Fig. 2.1. The final lens and Mu-metal shields are always earthed, and except for special applications, the specimen is also earthed; the electron multiplier input and first dynode are connected together, and are biased about 100 volts positive with respect to earth. Smith found that when he earthed the multipler input, the output current dropped to only 5% of the value obtained when the multiplier input was 100 volts positive. He also found that the multiplier output was a sensitive function of the specimen potential. From these two observations he surmised that secondary electrons are the major source of the multiplier output current (see Smith, 1956, p. 125).

2.2. The Energy Distribution of the Amplified Electrons.

As an initial experiment, Mr. Oatley suggested that the author should measure the energy distribution of the electrons contributing to the video signal, without appreciably altering the geometry or potential in the specimen chamber. Accordingly, three copper gauze grids were mounted immediately above the multipler input; the first and third grid were connected to the multiplier input and held at + 116 volts, the voltage of the second grid was variable. Fig. 2.2 shows the experimental geometry, and the video signal variation as a function of the second grid voltage. Since the amplifiers were linear, the video signal is directly proportional to the input current which is amplified by the electron multiplier. The black level (no input to the electron multiplier) is given by the horizontal line marked "beam off".

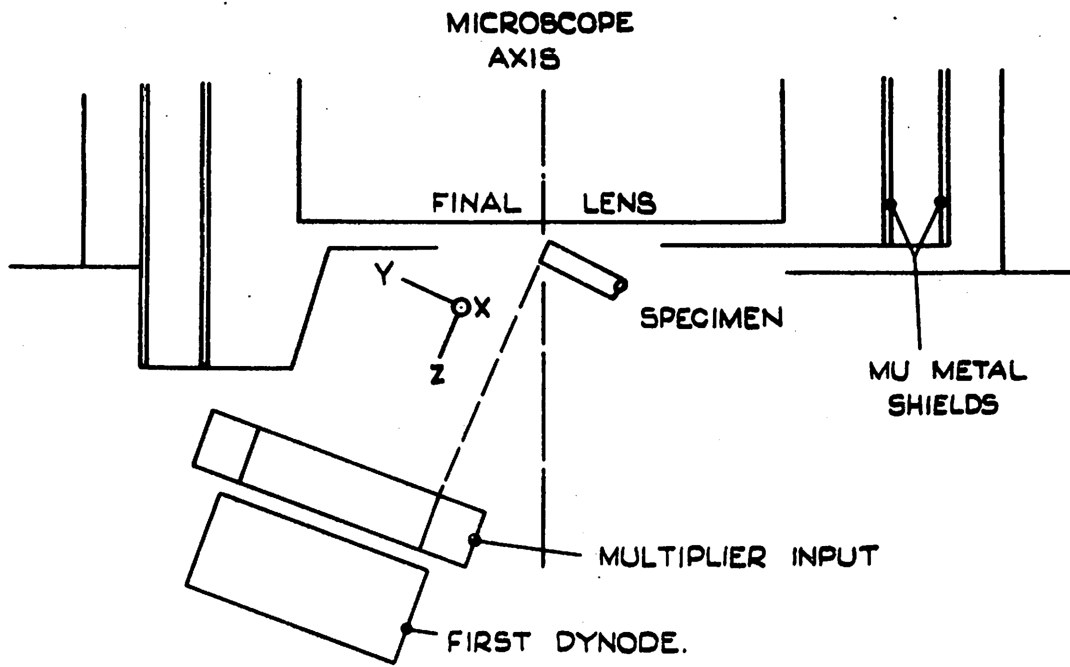

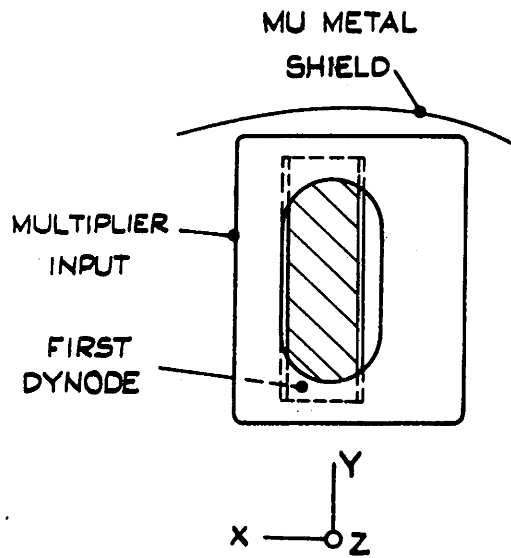

SMITH'S COLLECTION GEOMETRY
TWO VIEWS.

FIG. 2.1.

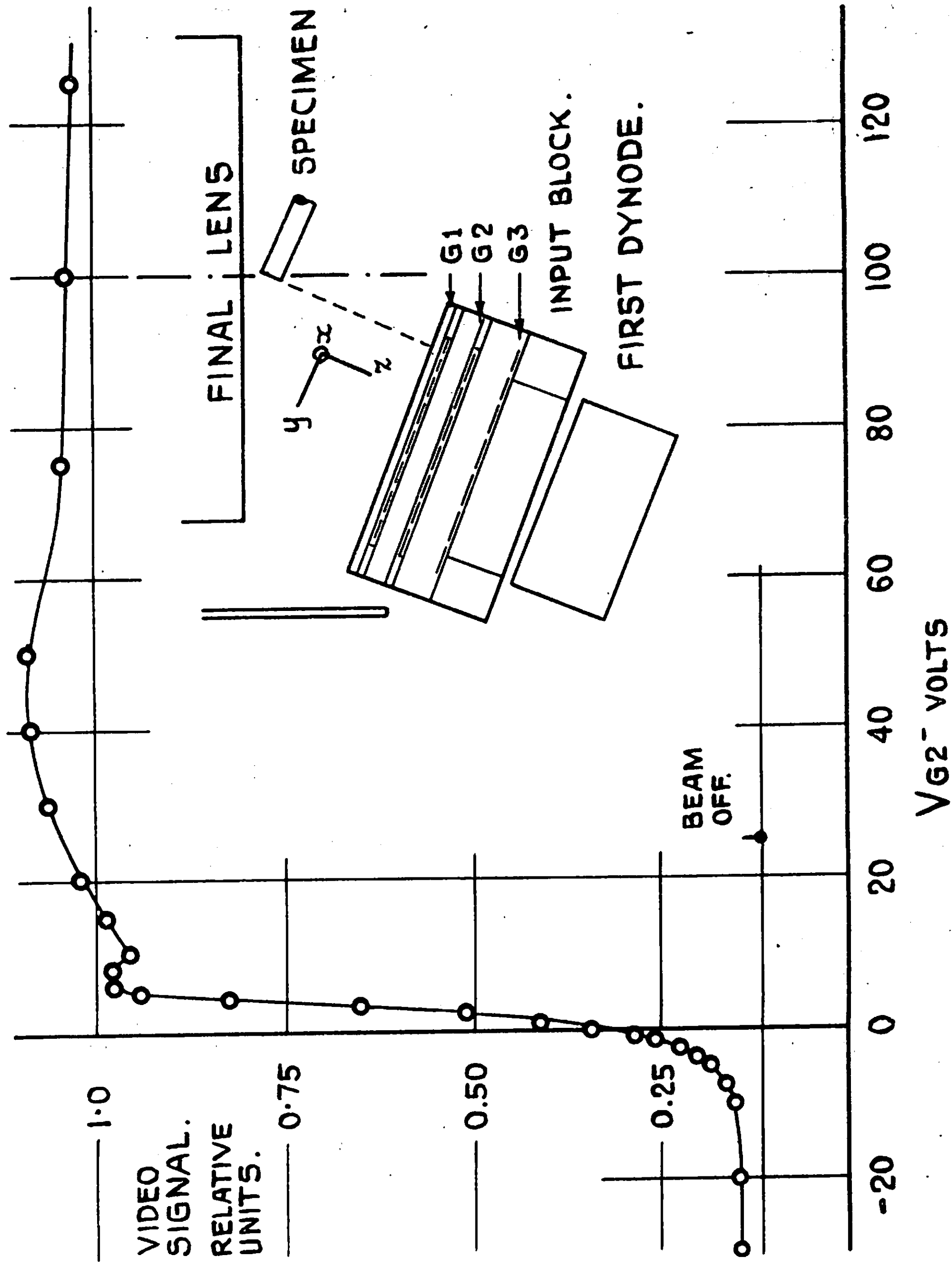

FIG. 2.2.

About 3% of the video signal comes from electrons with incident energies greater than 20 volts. About 90% of the video signal variation occurs in the range $-10 < V_{G2} < +10$, showing that most electrons contributing to the video signal have low energies. The exact form of this curve may be understood by realizing that the number of secondary electrons emitted from a plane surface at an angle θ to the surface normal is proportional to $\cos\theta$. (Jonker, 1951). In the geometry of Fig. 2.2, where the specimen normal is parallel to the multiplier input plane, half of the secondaries will therefore have component velocities toward the multiplier, and half will have component velocities away from it, increasing the observed energy spread. Although the copper gauze grids were etched in concentrated nitric acid to increase their porosity, they undoubtedly collected a certain number of electrons, especially when the second grid voltage was near zero, for transverse velocities are then comparable to the velocity toward the first dynode. The small dip at 10 volts, repeatable over four trials, may be due to a sudden decrease in the number of electrons which strike the second grid at grazing incidence, and excite secondaries which are subsequently collected. The rise in signal from 10 to 50 volts is believed due to secondary electrons from the second grid which strike the first dynode with appreciable energy. As the second grid voltage increases, the energy of these electrons at the first dynode decreases, with a corresponding decrease in the video signal.

2.3. Reflected Electron Images vs. Secondary Electron Images.

Smith (1956, p. 124) showed that by holding a scintillator near the specimen, where some of the reflected electrons would strike it, and by amplifying the resulting light with a photomultiplier, an image due only to reflected electrons could be obtained. In order to directly compare a reflected electron image with a secondary electron image, the author modified the specimen chamber so that identical areas of the specimen could be imaged by either the reflected or the secondary electrons. Fig. 2.3. shows the experimental arrangement. When the reflected electron image is desired, the scintillator is moved into position before the specimen, as shown in 2.3a. and 2.3b. When the secondary electron image is desired, the scintillator is retracted, as shown in Fig. 2.3c. In order to maximize the number of reflected electrons which are collected, without sacrificing light-pipe efficiency, the cylinder of plastic scintillator has been cut at the angle of total internal reflection, i.e., referring to Fig. 2.3d., $\beta = \sin^{-1}(\frac{1}{n})$, where $n = 1.54$ is the index of refraction of the plastic scintillator, Pamelon (private communication, Isotopes Development Ltd.).

Fig. 2.4a. shows two reflected electron micrographs of an etched surface of aluminium; secondary electron micrographs are shown in Fig. 2.4b. Note the sharper contrast in 2.4a. and the lack of detail in deep etch pits. It is evident that secondary electron images yield more information about rough specimens, which are the specimens

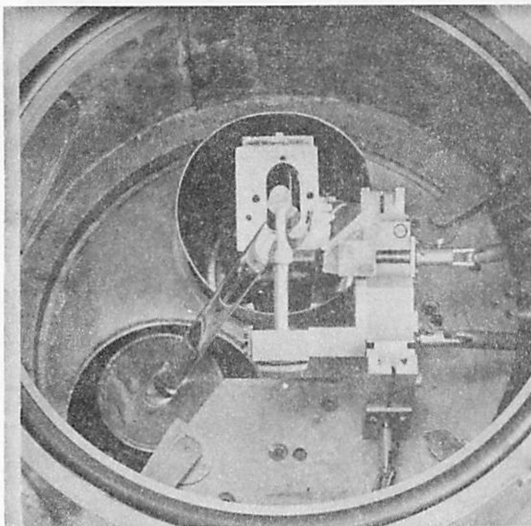

2.3a.

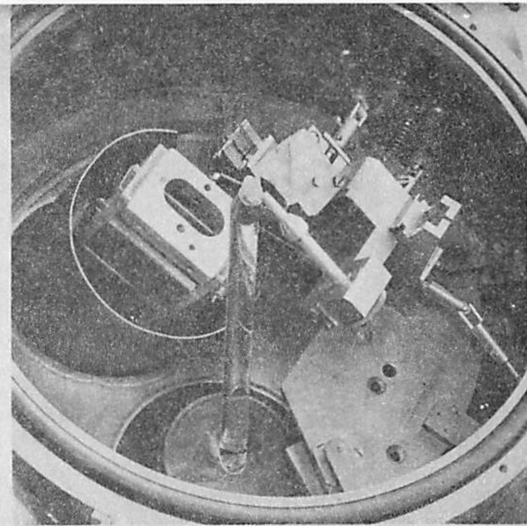

2.3b.

Scintillator positioned before specimen for reflected electron image.

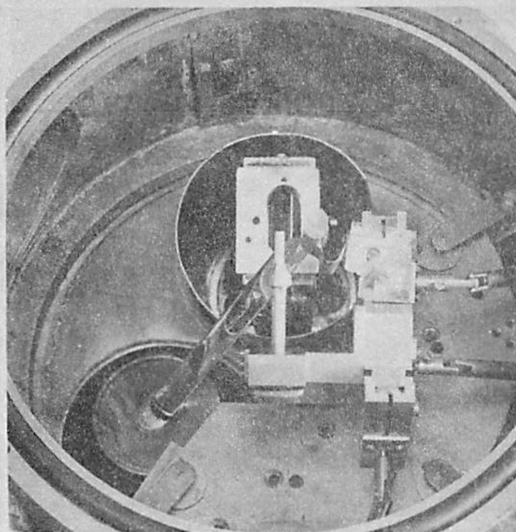

2.3c. Scintillator retracted for secondary electron image.

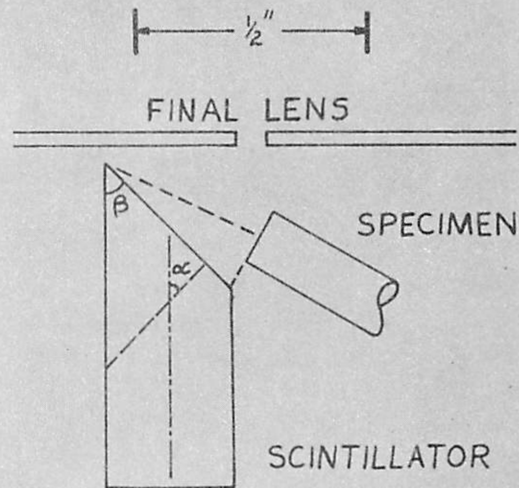

2.3d. Diagram of scintillator-specimen geometry.

Fig. 2.3. Secondary or Reflected Electron Collection Geometry.

M = 560

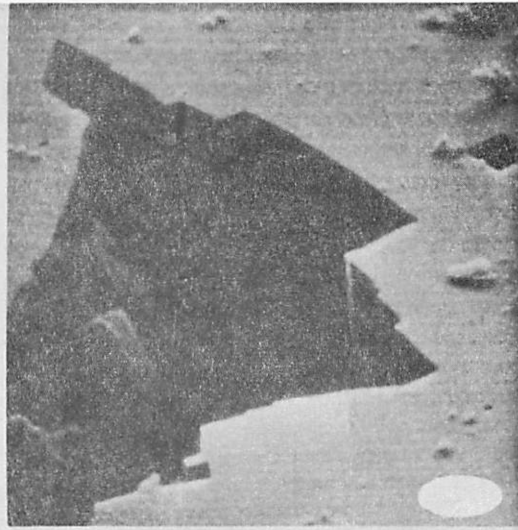

M = 1500

2.4a. Reflected Electron Micrographs of Etched Aluminium.

M = 1500

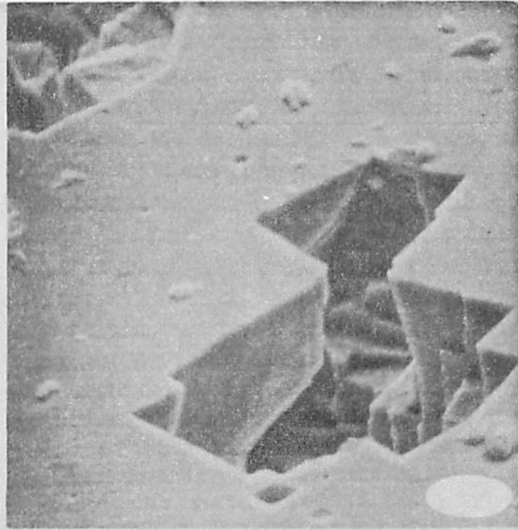

M = 1500

2.4b. Secondary Electron Micrographs of Etched Aluminium.

Fig. 2.4. Reflected Electron vs. Secondary Electron Images.

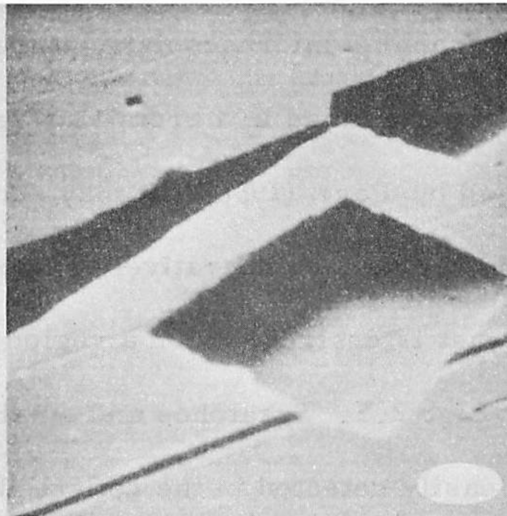

M = 1600

2.5a. Reflected Electron Micrograph of Etched Aluminium.

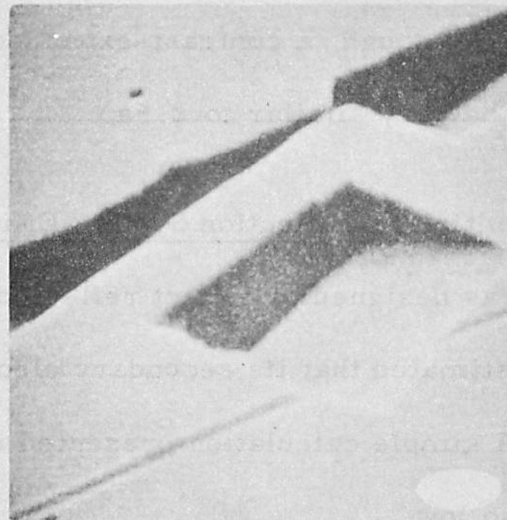

M = 1600

2.5b. Secondary Electron Micrograph of Etched Aluminium.

Fig. 2.5. Reflected Electrons vs. Secondary Electron Images.

of greatest interest to scanning microscopists, since smooth surfaces are easily replicated, or examined in a promising reflection instrument recently described by Page (1958). It may sometimes happen that a rough surface has certain comparatively smooth regions, and an image with more contrast is desired. Such a region of the same specimen is shown in Fig. 2.5. Scratches and small asperities on the surface are more easily detected in the reflected electron micrograph, 2.5a. The diffuse shadow in 2.5a. results from the large solid angle subtended by the collector, which gives a penumbral effect. The secondary electron image, Fig. 2.5b., is somewhat noisy, which decreases the detection probability of small contrasts; if the signal-to-noise ratio were high enough, a contrast-expanded secondary electron image would be very similar to 2.5a.

2.4. The Electron Multiplier Collection System Efficiency.

This system was designed to collect reflected electrons. Smith (1956, p. 81) estimated that its secondary electron collection efficiency was 0.2. A simple calculation presented in this section indicates why it was so low.

Fig. 2.6a. shows the equipotentials for this system, and Fig. 2.6b. shows typical secondary electron trajectories. (These figures were kindly provided by Mr. M. R. Barber at the author's request.) It is evident from the trajectories in Fig. 2.6b. that most secondary electrons emitted along the specimen normal enter the

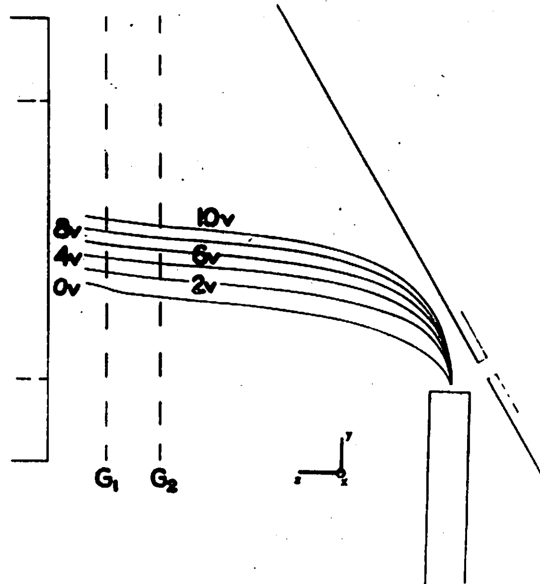

2.6b. Variable Energy Electron Trajectories, Electron Multiplier Collection Geometry.

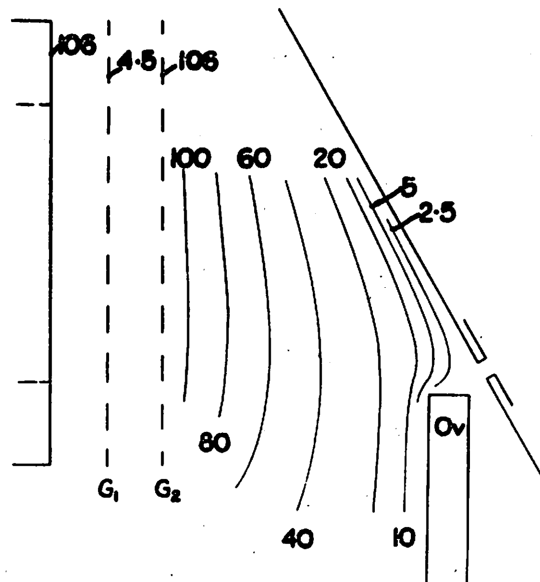

2.6a. Equipotentials of Electron Multiplier Collection System.

Fig. 2.6. Electrolytic Tank Traces.

multiplier. Other trajectory traces not shown here reveal that secondary electrons emitted in the y-z plane will enter the multiplier unless their initial velocity carries them to the final lens and they are collected by it. Since secondary electrons are assumed to leave the specimen with a cosine distribution and low energies, most secondaries emitted in the y-z plane enter the multiplier.

Because of symmetry there are no fields perpendicular to the y-z plane. If t is the secondary electron transit time between specimen and multiplier, and v_x is the electron's initial velocity in the x direction, then the transverse displacement at the multiplier is simply $x = v_x t$. The transit time t may be estimated by assuming that an electron emitted along the specimen normal finds itself in a uniform field toward the multiplier given by the multiplier voltage divided by the specimen-multiplier distance. Since Fig. 2.6a. shows the field is stronger near the multiplier, this value of t will be less than the actual value. Substituting the half width of the multiplier input for x, the maximum x component of energy which a secondary electron may have and still be collected is found to be ≤ 1.0 ev. This simple calculation indicates that the poor efficiency of this system is mainly caused by transverse velocities of the secondary electrons.

2.5. Limitations of the Electron Multiplier Collection System.

The low efficiency mentioned in the preceding section is a serious limitation of the electron multiplier collection system. This system is also inflexible; the multiplier input position can be altered only by making a new bottom plate for the specimen chamber, a costly, time-consuming job. In addition, the electron multiplier input must be about 100 volts positive, which means the output must be from 4 to 6 kv. above earth, and a floating valve head amplifier is necessary (see Smith, 1956, p. 86). This floating head amplifier and its associated power supply were a constant source of trouble during the author's early research. If the multiplier output could vary about earth potential, the head amplifier could be eliminated, and more important, a direct-coupled video amplifier could be used. Because of the long recording times necessary for a noise free micrograph, a direct-coupled amplifier would eliminate both sag, which occurred in the existing video amplifier, and the clamping circuitry, which proved troublesome on occasions.

2.6. Desirable Characteristics of a New Collector System.

After using the electron multiplier system for some months, it became clear that a new collector system was necessary for the envisaged work on contrast formation. The new system should have the following desirable characteristics. (1) It should be flexible,

permitting the specimen-collector geometry to be changed quickly and easily. (2) The change-over from transmission to reflection should be greatly simplified; the electron multiplier change-over took about 30 minutes, and the multiplier had to be removed from one container and inserted into another, a process which more than once damaged it. (3) The new system should collect almost all the secondary electrons, and introduce negligible noise in their amplification. (4) The video output should vary about earth potential, and should be large enough to be amplified by a valve amplifier without introducing additional noise. (5) The system should be capable of amplifying frequencies from 0 to about 1 Mc/s., and ideally it should be capable of recording a reflected electron image as well as a secondary electron image.

For collector currents of the order 10^{-11} to 10^{-12} amp., an electron multiplier preamplifier is essential for reasonably noise free, wide-band amplification. If the signal can be transformed into light, which is then amplified by a photomultiplier, the floating head amplifier can be eliminated. Zworykin, Hillier, and Snyder (1942) did this, but their low signal-to-noise ratio probably indicates that their system was not very efficient. McMullan suggested using a few stages of electron multiplication, then accelerating the amplified current onto a phosphor, and collecting the emitted light with a photo-multiplier, which can be operated with its collector near earth. The electron

multiplication was deemed necessary to avoid long time constants observed when phosphors are bombarded with minute current densities (McMullan, 1952, p. 115). Wells (1957, p. 30) showed that this system would work, but it is complicated, inflexible, and the phosphor is easily contaminated.

2.7. A Scintillator-Photomultiplier Collection System.

Preliminary tests showed that the plastic scintillator, Pamelon, had a conversion efficiency comparable with two fast phosphors available in the laboratory. Therefore a new collection system was designed around a hemispherically capped cylinder of Pamelon; the Pamelon was prevented from charging by an evaporated coating of aluminum approximately 700 A. thick. This coating also reflects the light generated by the incident electrons down the light-pipe (which is attached to the base of the Pamelon cylinder) to an EMI 6094B photomultiplier, whose output varies about earth potential. Reflected electron images are produced when the earthed scintillator is held near the specimen, as in Fig. 2.7a. When the scintillator is biased positively at the CRT anode potential of 7 kv., and placed a few centimeters from the specimen, the video signal is almost entirely due to secondary electrons. In this configuration, screening is sometimes necessary to avoid distortion of the specimen scan by the electric field from the scintillator. The standard arrangement, arrived at by experiment, is shown in Fig. 2.7b.

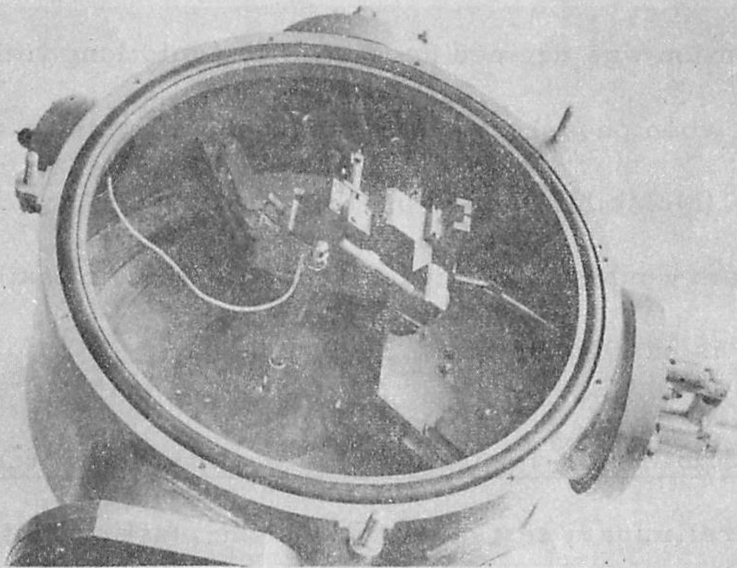

2.7a. Reflected Electron Collection.

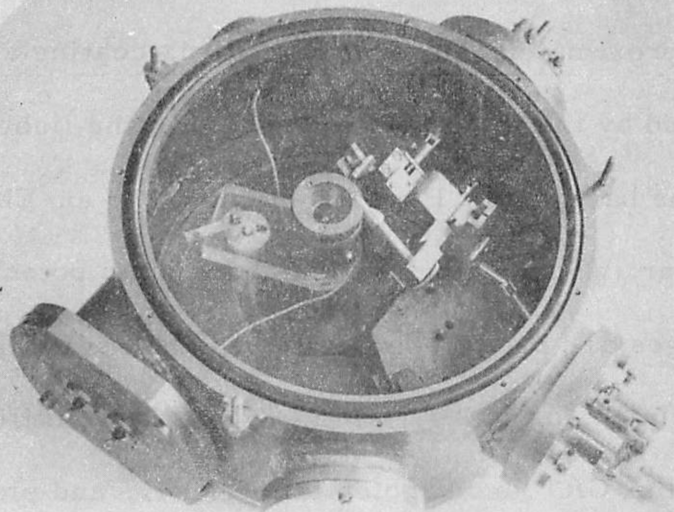

2.7b. Secondary Electron Collection.

Fig. 2.7. Scintillator-Photomultiplier Collection System.

This system satisfies all the conditions mentioned in the preceding section. The light-pipes are cut from standard quarter-inch diameter perspex rod; they can be bent to any desired shape by gently heating them in a bunsen flame, bending them, and allowing them to cool; this process takes about three minutes. The flexibility of the system is increased by using a series of light-pipes, joined by short brass tubes; the high index of refraction light path is preserved by using Apiezon B oil at the perspex-perspex interface, a small hole in the brass tube allowing pressure equalization as the specimen chamber is evacuated. The Pamelon button, as the hemispherically capped cylinder is called, is connected to the light-pipe by another brass tube, which contacts the aluminum coating, and is connected to the 7 kv. CRT supply through a resistor-condenser filter and current limiting network. The system is changed from reflection to transmission by inserting a different light-pipe; this operation takes about two minutes. Fig. 2.8. shows several of the light-pipes used during the author's investigations into contrast formation. A brass connecting tube is attached to H, and a Pamelon button is shown in the foreground. The shoulders shown on light-pipes A, B and J rest against the outside wall of the specimen chamber. The light-pipe enters the specimen chamber through a quarter-inch hole, fitted with an O-ring vacuum seal. Thus the photomultiplier can be outside the vacuum.

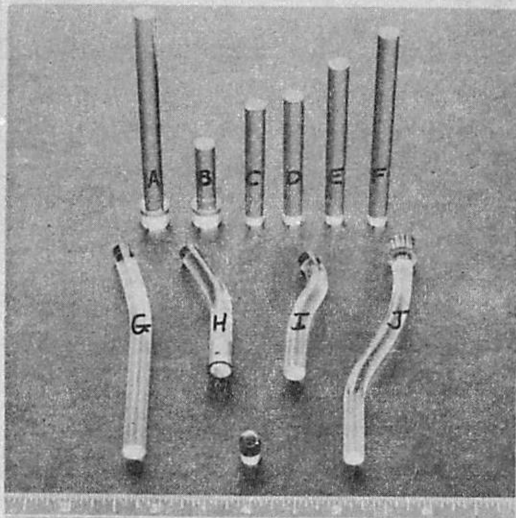

Fig. 2.8. Light-pipes.

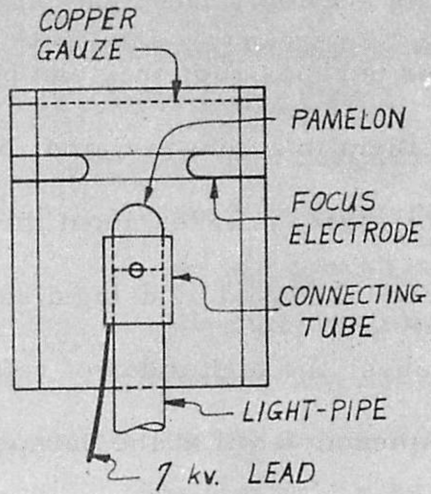

Fig. 2.9. Diagram showing Collector-Scintillator Geometry.

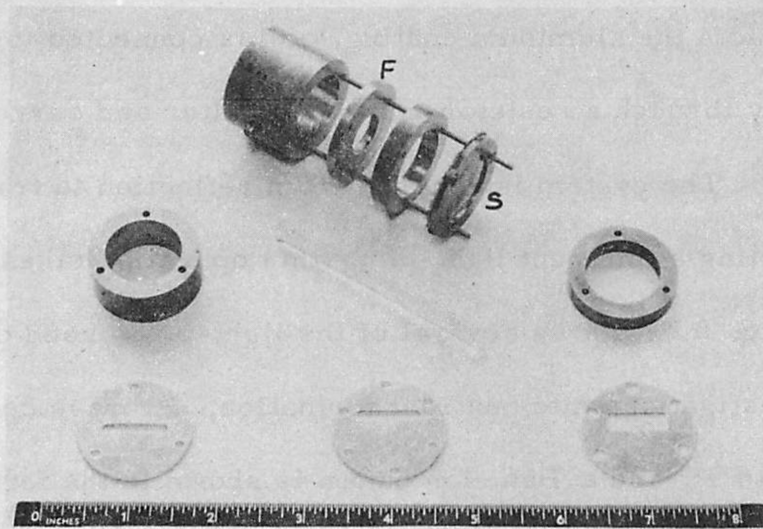

Fig. 2.10. Exploded View of Collector.

The collector, shown in Fig. 2.7b., screens the specimen from the scintillator, and screens the scintillator from stray electrons and negative ions which would otherwise be attracted to it. The electrons attracted to the collector by its 200 volts positive bias penetrate a piece of etched copper gauze, and are focused onto the Pamelon button to some extent by the focus electrode shown in Fig. 2.9. This figure shows the standard collector-scintillator geometry. However, in keeping with the proposed study of contrast formation, the collector was designed for maximum flexibility; an exploded view is shown in Fig. 2.10. The toroidal sections are held on three lengths of studding. The height of the collector with respect to the rest of the specimen chamber may be altered by adding or subtracting one of the sections. The copper gauze screen S and the focus electrode F are marked for clarity. The electrodes in the foreground are shields which were placed over the collector input in connection with potential detection studies.

The quoted fluorescent decay time for Pamelon is 8×10^{-9} sec. This system will therefore amplify frequencies well above 10 Mc/s.

2.7.1. <u>The Scintillator-Photocathode Conversion Factor</u>.

If the number of electrons produced at the photocathode is greater than the number striking the scintillator, little noise is introduced in the electron-light-electron conversion. Following Birks

(1953, Chapter 2), the number of electrons produced at a photocathode by one electron incident on the scintillator is:

$$n = \frac{E_1 \; A \; C_{ip} \; T_p \; G \; C_{pe} \; f(\nu_p)}{E_p} \; . \qquad (1)$$

Where E_1 = energy of incident electron, ev.

A = fraction of E_1 dissipated in the scintillator.

C_{ip} = energy conversion efficiency into photons of average energy E_p.

T_p = transparency of scintillator and light-pipe.

G = fraction of the photons which reach the photocathode.

C_{pe} = conversion efficiency of photocathode.

$f(\nu_p)$ = spectral response of photocathode to photons of energy $h\nu_p$.

E_p = average energy of photons, $\frac{1.25 \times 10^4}{\lambda \; (A.)}$ ev.

From the Thomson-Whiddington Law, the energy of the electrons after penetrating the metallic film is:

$$E_1 = \sqrt{E_o^2 - ax} \qquad (2)$$

where E_o = incident energy of electron, ev.

$a = 4 \times 10^{11} \; \rho \; ev^2/cm.$ (Terrill, 1923).

x = thickness of metallic film, cm.

In this case, $\rho = 2.7$, $x = 7 \times 10^{-6}$ cm., and $E_o = 7,000$ ev.

Therefore, $E_1 = 6,400$ ev. All this energy is dissipated in the scintillator, so A = 1. Birks (p. 79) states that anthracene has a conversion efficiency of 0.04; for Pamelon, which is about half as efficient, $C_{ip} \approx 0.02$. Both perspex and Pamelon are very transparent, so $T \approx 1$; it is shown in Appendix 1 that $G \approx 1$. Birks (p. 24) states that 10^{-6} amp/lumen is equivalent to 0.0025 electrons per photon at the wavelength in question, and the specified minimum sensitivity of the 6094 B photomultiplier used (an old vintage) is 20×10^{-6} amp/lumen, so $C_{pe} \geq 0.05$. From the photomultiplier spectral response curve $f(\nu_p) = 0.93$, and for the emission wavelength of Pamelon, 4600 A., $E_p = 2.72$ ev. Substituting all these values into equation 1,

$$n \geq 2.2 \tag{3}$$

The photocathode conversion efficiency is probably better than stated above, but anthracene and Pamelon have lower conversion efficiencies at these low electron energies. These two errors tend to compensate, and from the value of n calculated, it is safe to assume that little noise is added by the conversion process.

2.7.2. Relative Light Output of Pamelon.

Fig. 2.11. shows the relative light output of an aluminized Pamelon button as a function of incident electron energy. To obtain this curve, the scintillator was bombarded with a defocused,

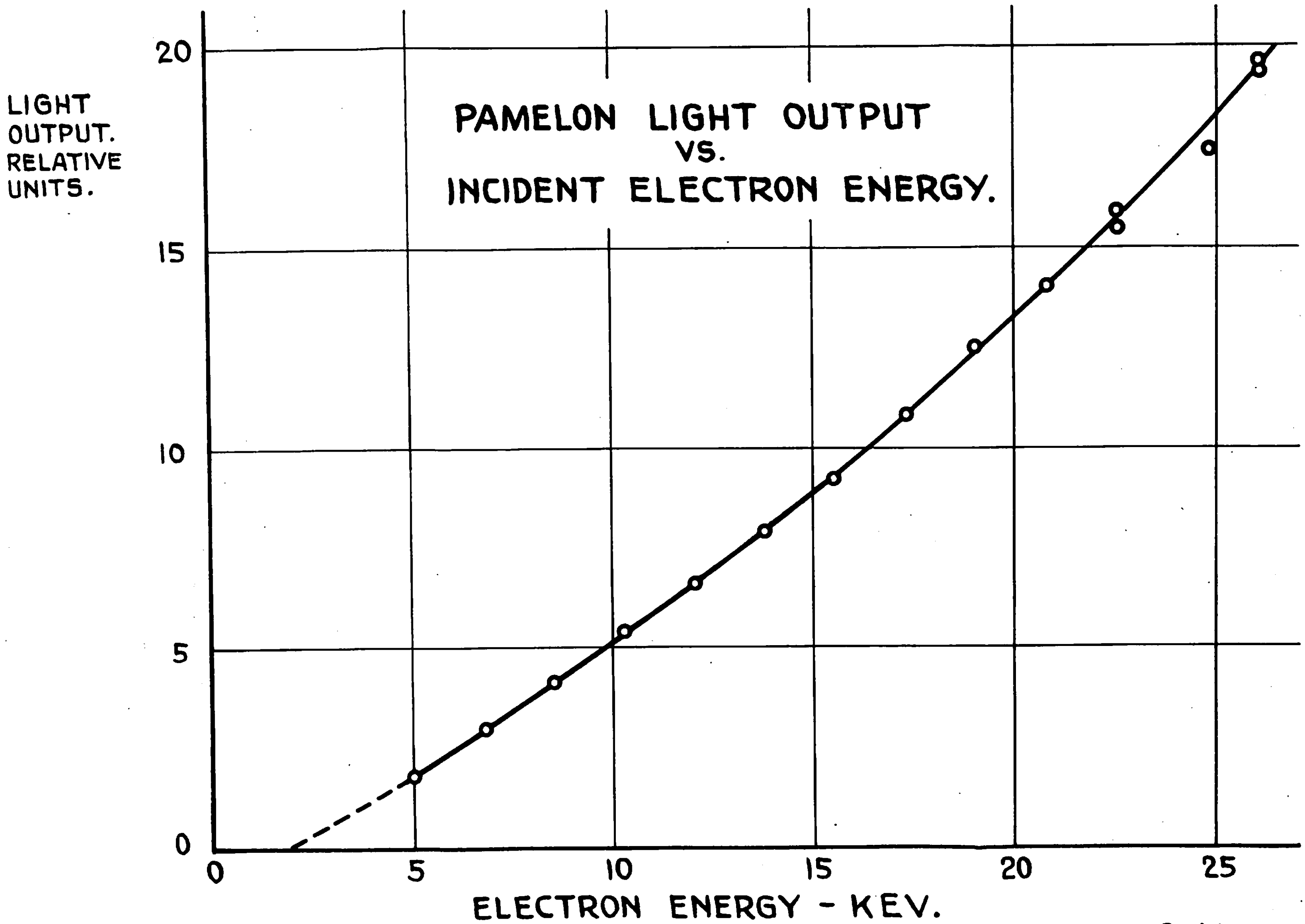

FIG. 2.11.

constant current 5 kv. primary electron beam. The scintillator voltage was varied from 0 to 7 kv., and the video output measured at 1.4 kv. intervals. When the scintillator voltage equalled 7 kv., the energy of the electrons striking the scintillator was 12 kev. At this point, the scintillator voltage was decreased to 0, and the primary beam voltage was increased to 12 kv. Because the primary beam current increased during this change, the photomultiplier voltage was altered to compensate for the change in primary beam current, and the video output at 12 kev. incident energy remained the same. This process was repeated twice to cover the energy range from 5 to 26 kev.

If the curve is extrapolated to zero light output, the energy intercept is 2.2 kev. The mean energy required for an electron to penetrate a 700 A. aluminum film is 2.75 kev. by the Thomson-Whiddington Law quoted above, but a recent empirical formula by Young (1957) gives the energy intercept as 1.4 kev. The observed energy intercept falls between these two values.

Limiting in the scintillator was noticed only when the primary beam was focused on its surface; the current density then is of the order of 1 amp/sq. cm., and it is not surprising that a small volume of a material designed to count a few hundred electrons per second should balk at 10^8 electrons per second, a factor of 10^6 greater.

2.7.3. The Photomultiplier Gain.

The relative photomultiplier gain was obtained by allowing a constant current defocused primary beam to fall on the Pamelon button, and measuring the output current of the photomultiplier as the total dynode voltage was varied from 1.1 to 2.2 kv. The resulting curve, shown in Fig. 2.12., may be expressed analytically with only a few percent error as $I \propto V^{7.2}$. The manufacturer states that the variation should be approximately $I \propto V^{8}$, therefore the gain per stage of the multiplier used is probably slightly below specification. It is often useful to compare the signal level at the scintillator for different collection geometries; this is achieved by knowing the photomultiplier output current, the total dynode voltage, and Fig. 2.12.

2.7.4. The Collection Efficiency.

As the absolute gain of the photomultiplier is not known, the collection efficiency cannot be calculated directly. Therefore, it was measured in the following manner. The earthed scintillator was bombarded by a 7 kv. defocused beam of electrons. The current striking the scintillator I_s was measured by an electrometer connected to a movable Faraday cage; the output current of the photomultiplier I_p was also measured, at a known value of total dynode volts, V_T. The ratio of these two currents, I_p/I_s equals the gain of the system, G. Next, a 100 micron copper aperture was mounted on a partially

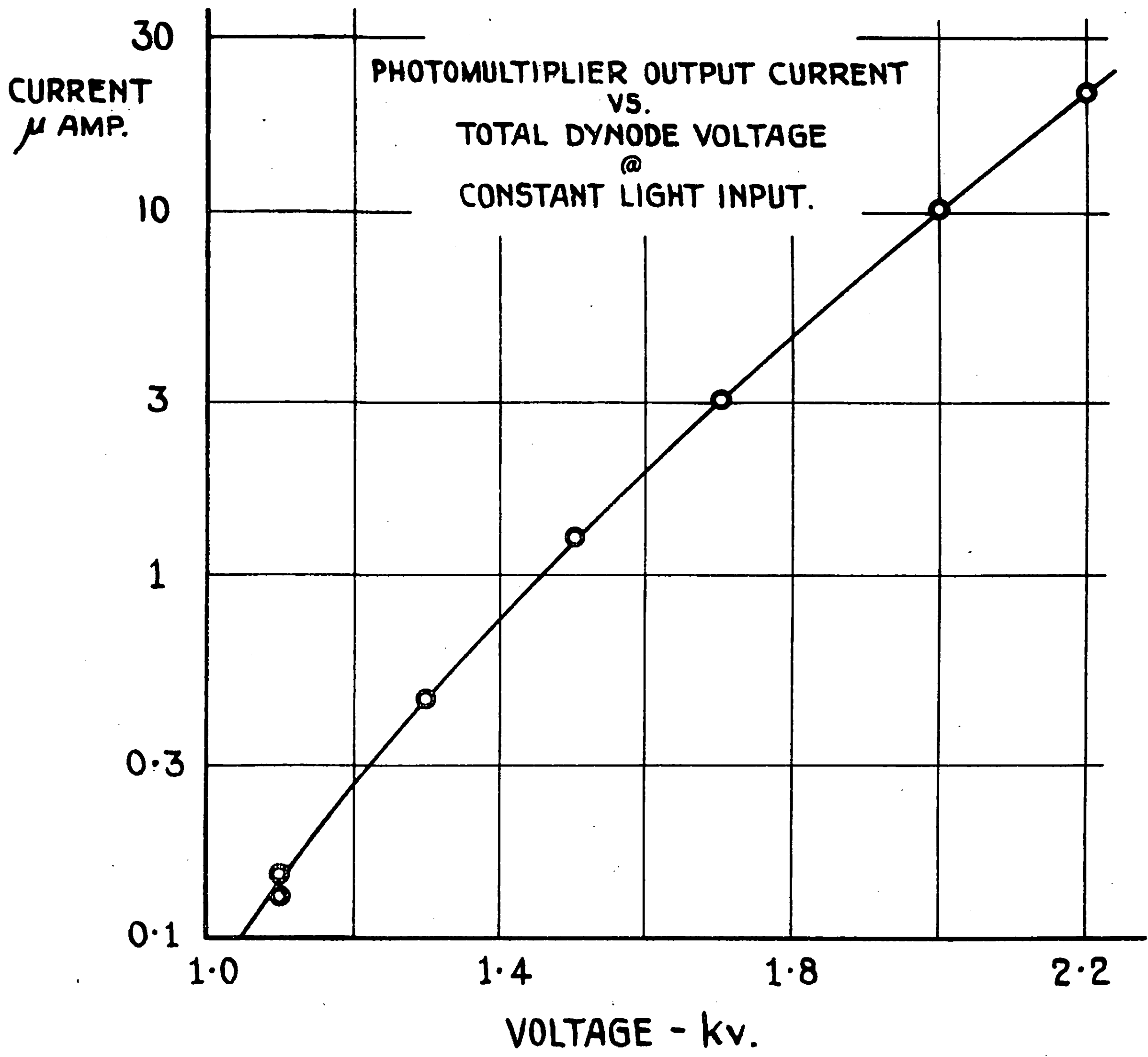

FIG. 2.12.

drilled out specimen stub, as shown in Fig. 2.13. This aperture was then mounted in the microscope, at a grazing angle of 35° to the primary beam. A micrograph of the aperture in this position is shown in Fig. 2.14. In order to measure the current flowing to the specimen, the insulation resistance to other electrodes in the specimen chamber was kept greater than 10^{12} ohms. The electrometer was connected to the specimen, and by focusing all the primary beam through the hole in the aperture, the primary beam current I was measured. By moving the specimen laterally, the primary beam struck the aperture at one side of the hole; and the current to the specimen, I_1, was measured. Therefore the current leaving the specimen (for constant primary beam current) was $\Delta I = I - I_1$. The collection system was arranged in the standard manner shown in Fig. 2.7b.; the collector potential was set at + 200 volts, the scintillator bias at + 7.0 kv, and the photomultiplier total dynode voltage was again set to V_T. The current striking the scintillator was then found by measuring the photomultiplier output current, I_p, and dividing it by G. Fig. 2.15. summarizes the results of this measurement, which was repeated several times with different light-pipes, to check the effect of joints in the light-pipes, and the vertical position of the scintillator in the collector. Trials A and B are identical, and provide a check on the experiment. They show the accuracy of the ratios I_s/I and $I_s/\Delta I$ is probably about 5 to 10%. Trial C shows that the efficiency is increased if one

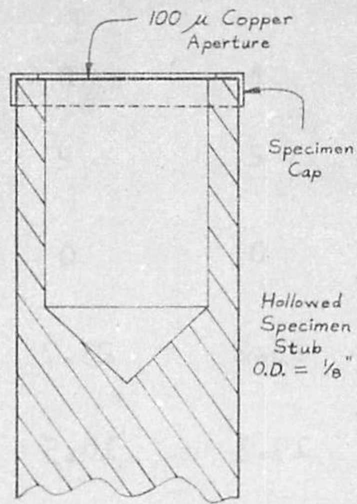

Fig. 2.13. Diagram of Aperture on Hollow Specimen Stub.

M = 400

Fig. 2.14. Micrograph of 100 micron Copper Aperture.

COLLECTION EFFICIENCY DATA

Trial	A	B	C	D
Number of Joints	2	2	1	2
Relative height	0	0	$-\frac{1}{32}$"	$-\frac{1}{8}$"
I $\mu\mu$amp. measured	25.2	23.7	22.5	20.9
Δ I $\mu\mu$amp. measured	19.3	16.5	16.1	14.6
I_s $\mu\mu$amp. calculated	25.2	22.3	36.7	23.2
I_s / I	1.0	0.94	1.63	1.11
I_s / Δ I	1.30	1.35	2.28	1.59

Collector - 200 volts

Photomultiplier - 1100 volts

Primary Beam - 16,000 volts

Magnification - 200 times

Grazing Specimen angle θ - 35°

Scintillator - 7,000 volts

TABLE 2.1.

FIG. 2.15

oil joint is removed, and the scintillator position is lower. Trial D shows that an even lower scintillator position is more efficient than the initial position, but because of the double oil joint in trials A, B and D, they are not directly comparable to C. All trials show that more electrons strike the scintillator than leave the specimen. Therefore, some secondary electron multiplication must take place before the scintillator, probably from the focusing electrode shown in Fig. 2.9. The amount of electron multiplication is somewhat surprising, since many electrons entering the collector must strike the scintillator directly. It seems safe to assume that most secondary electrons leaving the specimen enter the collector; some of these strike the focusing electrode at grazing incidence, emitting several secondaries which then are accelerated to the scintillator. The data in Fig. 2.15. show the height of the scintillator in the collector is fairly critical, if optimum performance is to be achieved, and the oil joints probably transmit about 70 to 80% of the light incident upon them. This last factor will somewhat modify the calculation in Section 2.7.1., but not the conclusion.

2.7.5. Analysis of the Amplified Electrons.

In Section 2.2. it was concluded from an experiment that secondary electrons contribute over 95% of the video signal. A complementary experiment was performed with the new collector

system, by placing a grid near the specimen, as shown in Fig. 2. 16a. The top of the grid was less than half a millimetre from the final lens, and the grid, specimen, and collector potentials could be varied independently. Fig. 2. 16a. shows the video signal variation with grid voltage. If the grid is a few volts positive, all the secondary electrons from the specimen are accelerated through the grid, and are collected. As the grid voltage decreases, the video signal falls because fewer electrons penetrate the grid; i. e., some electrons with initial velocities away from the grid will strike the final lens. As the grid voltage becomes negative, low energy secondaries can no longer penetrate it. For grid potentials below - 20 volts, the video signal decreases slowly; about 30% of the video signal is caused by electrons from the specimen with energies greater than 20 volts. This last observation is verified in Fig. 2. 16b., where the grid was earthed, and the specimen potential varied. In this case, the video signal is constant for specimen potentials exceeding about 20 volts, and is about 35% of the earthed specimen value. (Note that the two curves were normalized in slightly different ways).

These curves can be explained in terms of secondary electrons produced by reflected electrons striking the final lens at grazing incidence. When the grid is earthed, this component of the collected secondary electrons should remain constant as was observed in Fig. 2. 16b., for the final lens-collector region is screened from the

VIDEO SIGNAL vs GRID VOLTAGE
SPECIMEN VOLTS — 0
COLLECTOR VOLTS — 220

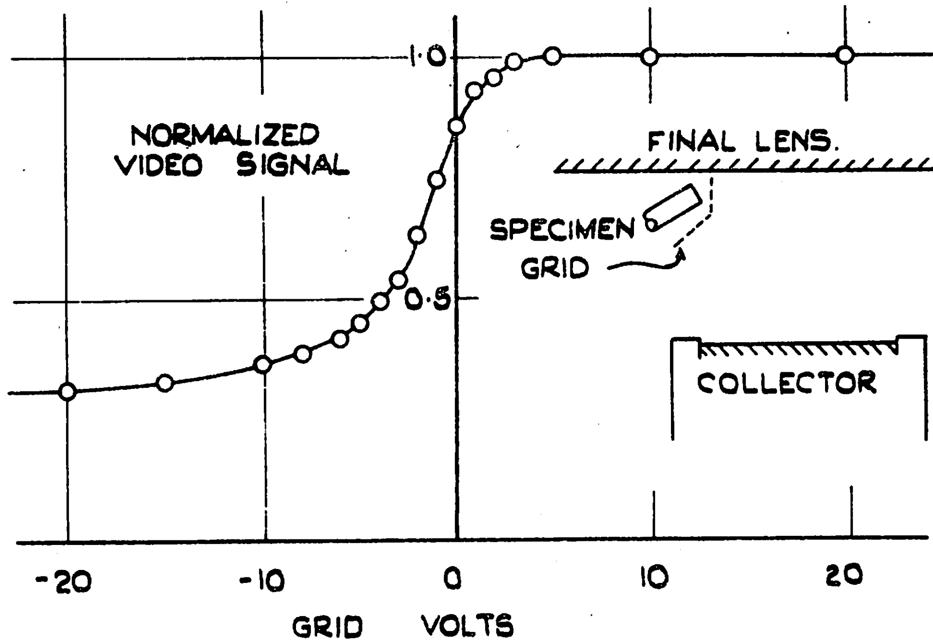

FIG. 2.16a.

VIDEO SIGNAL vs SPECIMEN VOLTAGE
GRID VOLTS — 0
COLLECTOR VOLTS - 220

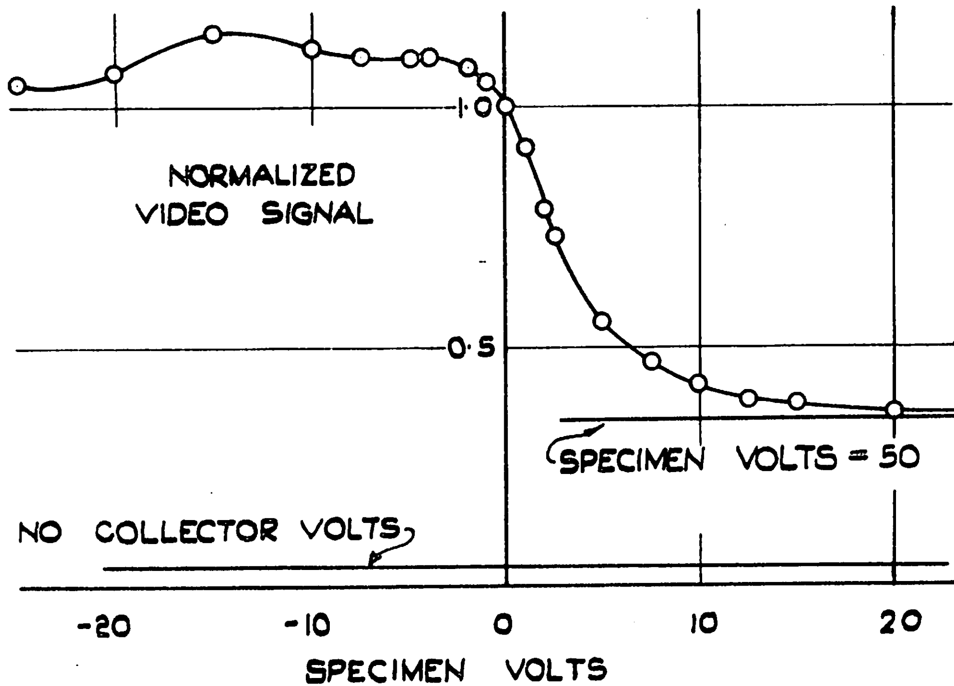

FIG. 2.16b.

specimen. As the grid potential becomes more and more negative, the number of secondary electrons from the final lens which enter the collector should decrease, for the negative grid will cause some of them to miss the collector. This was observed experimentally; the normalized video signal was 0.31 at V_{grid} = - 20 volts, 0.27 at - 30 volts, 0.23 at - 50 volts, and 0.20 at - 75 volts. This rather slow decrease suggests that some of the reflected electron induced secondaries may have come from the grid itself.

If the grid were not present, it is estimated that about 5% of the video signal is due to reflected electrons entering the collector, not more than 30% is due to secondary electrons excited by reflected electrons, and not less than 65% is due to secondary electrons from the specimen itself.

It is worth noting that if two adjacent areas of the specimen are at different potentials, for example, 0 and 2 volts respectively, and the grid is earthed, a contrast caused by this potential difference will be observed between these two areas on the CRT screen.

2.7.6. Video Signal Variation with Angle of Incidence.

Fig. 2.17. shows the variation of video signal as the angle between the primary beam and the specimen surface is varied. Selected smooth areas on an etched surface of high-purity aluminium were bombarded by the primary beam at different incidence angles to obtain this curve. The solid curve shows the normalized cosine

VIDEO OUTPUT
VS.
SPECIMEN ANGLE
PRIMARY BEAM CURRENT HELD CONSTANT
O EXPERIMENTAL POINTS.

collector	200 volts
primary beam energy	15 kev.

NORMALIZED
VIDEO
OUTPUT

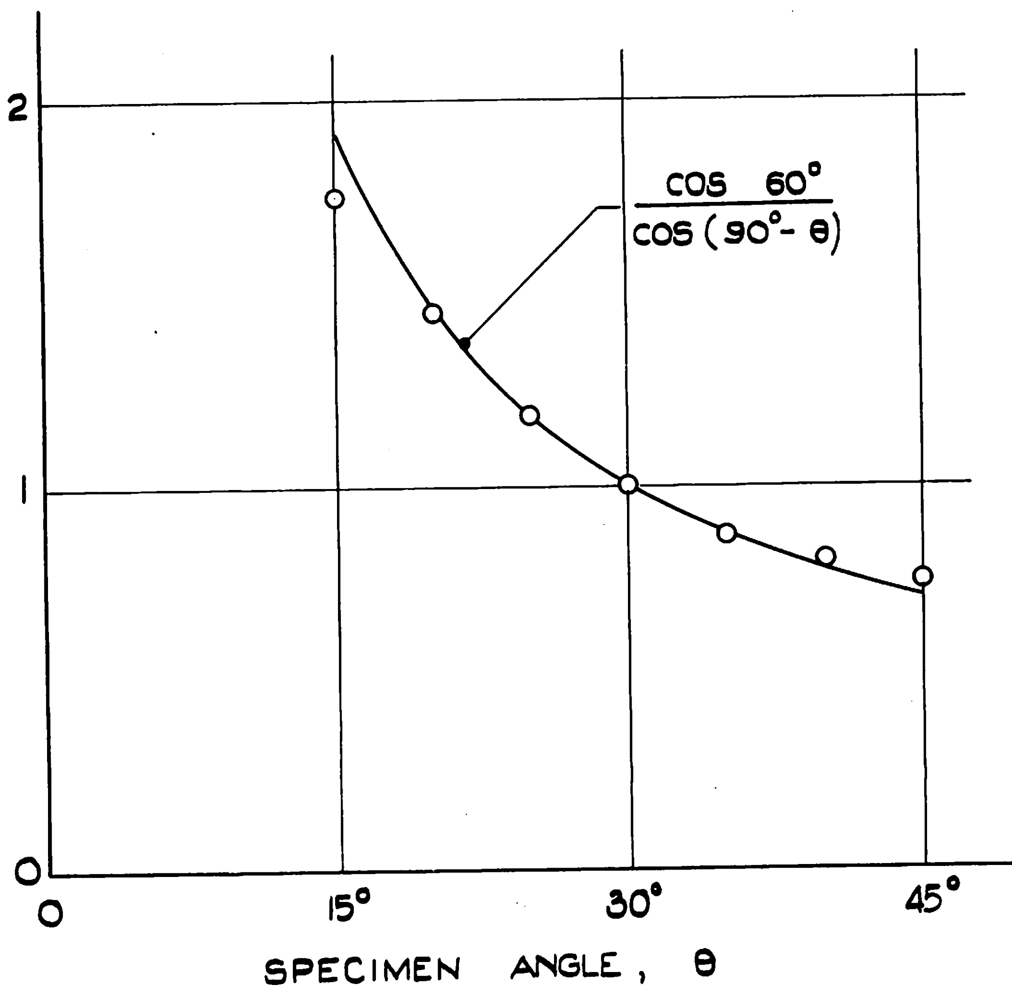

FIG. 2.17

variation which would be expected on the basis of Jonker's work (1952). Muller (1937) found appreciable deviations from this variation for small values of 0, and when the results of the previous section are considered, the agreement shown here seems surprising also, for the number of secondary electrons induced by reflected electrons will vary somewhat as the specimen angle is altered (McMullan's thesis Figs. 8.6. - 8.8. lead us to expect this). The curve of Fig. 2.17. is to be interpreted as an experimental curve which can be closely approximated by a cosine variation; it should not be interpreted as a justification for the cosine variation law of simple secondary emission theories.

2.8. Focusing at High Magnifications.

One great advantage of the present scanning electron microscope over previous models is the CRT display, which permits visual focusing. At the highest present resoltuion, the noise on the visual display introduces an uncertainty into visual focusing; this uncertainty will increase as the microscope is pushed to still higher resolutions, and therefore smaller spot sizes. Zworykin, Hillier, and Snyder (1942, p. 20) focused their microscope by peaking the high frequency component of the video signal, but this method is ineffective when the signal-to-noise ratio is low.

While performing the measurements reported in the previous sections, a 10 to 20% decrease in video signal was observed as the magnification was increased from 200 times to 200,000 times. This

decrease also was observed as the microscope was varied in and out of focus at 200,000 times magnification, the minimum in the video signal being observed when the microscope was in focus. When the primary beam makes an angle with the specimen normal, and is in best focus at the centre of the scanned area, the current density striking (and leaving) the specimen will vary across the scanned area, being higher in the centre than at the top and bottom edges. For a constant spot size, the mean current density leaving the specimen will decrease with the magnification. Similarly, when the beam is varied in and out of focus, the maximum current density striking (and leaving) the specimen also occurs at best focus. Calculation shows that the relatively high secondary electron current density leaving the specimen in the fields shown in Fig. 2.6. may well be reduced by space charge, the larger the current density leaving the specimen, the larger the reduction in collected current.

The observed decrease in video signal may be an important method of focusing the scanning microscope at very high magnifications, for the current density in the final spot will stay constant even if the spot size decreases (because the angular aperture α is now near the optimum value for high resolution work). This method of focusing may fail if secondaries are emitted over a larger area than is struck by the primary beam (see section 5.6.). Experiments with smaller spot diameters will determine the value of this technique.

CHAPTER 5.

THE SECONDARY ELECTRONS.

Before discussing contrast in terms of the secondary electrons (energy $\leq$ 50 ev), a brief review of secondary emission is presented. Certain measurements reported in the literature some years ago are given new interpretations using more recent knowledge of reflected electrons. These interpretations lead to a better understanding of contrast and an estimate of the probable ultimate resolution obtainable with the scanning electron microscope.

5.1. Elementary Theory of Secondary Emission.

The elementary theory of secondary emission qualitatively predicts the correct form of the δ vs. E_o curve (where E_o is the primary electron energy). This theory assumes that the primary electrons are incident normal to the target's plane surface, that they penetrate the material in a straight line along the axis of incidence, that the number of secondaries produced in an incremental path length, dx, is proportional to the energy loss of the primary electrons in that incremental length, and that this energy loss can be found from the Thomson-Whiddington Law. If a secondary electron is produced at

depth x, the probability that it will escape from the target decreases exponentially with x. This theory neglects all scattering; since the secondary emission coefficient δ ($= r + \delta_s$) depends partly on large angle scattering through r, this theory should be expected to predict the properties of δ_s, not δ.

The number of secondary electrons produced at depth x can be written, following Dekker (1957, p. 424) as

$$n(x) = \frac{c' \rho}{2 E_e E_o} (1 - \frac{x}{R})^{-\frac{1}{2}} , \quad (1)$$

where E_e is the average excitation energy required to produce a secondary, E_o is the primary energy, R is the range, and c' is the constant in the Thomson-Whiddington Law written in its energy form:

$$E^2 = E_o^2 - c' \rho x. \quad (2)$$

It is evident from (1) that n(x) increases as the electron energy decreases, i.e., as E_o decreases and x increases. If f(0) is the probability of escape of a secondary electron produced very near the surface, the probability of escape from depth x can be written:

$$f(x) = f(0) \exp(-x/L), \quad (3)$$

where L may be taken as the mean range of the secondaries. In general, δ may be written as the integrated product of f(x) and n(x),

$$\delta = \int n(x) \cdot f(x)\, dx. \tag{4}$$

For very low energies, $R << L$, Dekker shows that

$$\delta = f(0)\, \frac{E_o}{E_e}\,; \tag{5}$$

for very high primary energies, $R >> L$, $n(x)$ is approximately independent of x, and it follows that

$$\delta = \frac{c'\,\rho\, L}{E_e\, E_o}\, f(0). \tag{6}$$

It is apparent that if δ is increasing with E_o at low E_o, and is decreasing with E_o at high E_o, there must be a maximum δ at an intermediate value of E_o. Several authors have derived universal curves of δ vs. E_o following this general treatment. While these curves are qualitatively the same, the one derived by Jonker (1952) shows somewhat better agreement with experiment, and is plotted in Fig. 5.1. Jonker (1954) has shown experimentally that clean metals, with smooth, plane surfaces, do approximately follow a universal curve of secondary emission, if δ is normalized to δ_{max}, and E_o is normalized to the primary energy of maximum yield, $E_{o_{max}}$. The experimental curve is also plotted in Fig. 5.1. It is apparent that the theoretical curve falls off much faster at higher primary energies than the experimental curve.

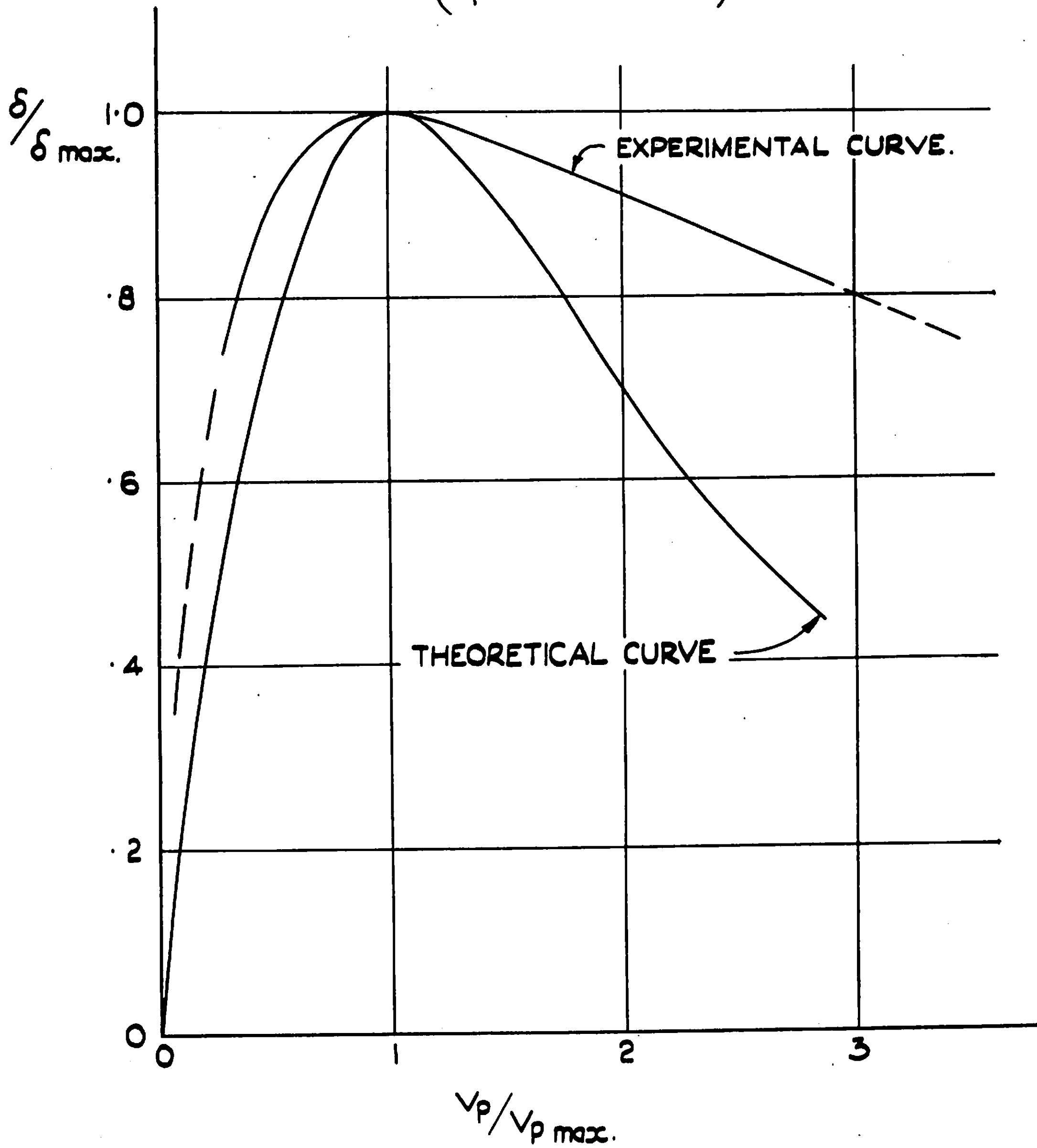

FIG. 5.1.

5.2. Variation of δ with Angle of Incidence.

When the primary beam makes an angle β with the target normal, Jonker (1954) has shown theoretically that if both the ordinate and abscissa of the universal curve are multiplied by $\sqrt{\cos\beta}$, the curve should remain unaltered. With all the targets he tested, the experimental curve followed this predicted behaviour. For high primary energies, (6) shows that at normal incidence, $\delta \propto 1/E_o$; therefore at constant E_o and angular incidence, β,

$$\delta \propto \frac{1}{\cos\beta} \tag{7}$$

Jonker's data extends up to primary energies about three times the primary energy of maximum yield, $E_{o_{max}}$, which is typically in the range $250 \text{ ev} \leq E_{o_{max}} \leq 1 \text{ kev}$.

5.3. Angular Distribution of Secondary Electrons.

Jonker (1957) has very carefully measured the angular distribution of the secondary electrons as a function of their energy. For all energies except the lowest, he found the angular distribution given by a cosine law, both for polycrystalline and single crystal targets. Below energies of about 1 ev., fewer electrons are emitted normal to the surface than would be predicted by a cosine law. In this experiment his 500 volt primary beam was incident normal to the target surface. Earlier work by Jonker (1951) showed that when the

primary beam is incident at an angle β to the specimen normal, the secondary electrons with energies less than 10 ev. are emitted with a cosine distribution for primary energies up to 450 ev. In his 1957 paper, Jonker argues that these results mean that the mean free path of the secondary electrons inside the metal must be small compared with the penetration depth of the primary electrons.

5.4. The Mean Depth of Origin of Secondary Electrons.

The range L which appears in equation (3) is an indication of the mean depth of origin of the secondary electrons when the range $R >> L$. Becker (1929) reported that for gold, L was about 100A, and for nickel, 66A. A more recent report by Sternglass and Wachtel (1955) states that $L \leq 20A$ for gold, however.

Copeland (1940) in some careful experiments measured δ as a function of primary energy for different thickness platinum films evaporated onto aluminium. He plotted δ vs. the number of evaporated atomic layers of platinum on the aluminium, showing a series of curves at different primary energies. All his curves have the same general shape: there is a sharp drop in δ between 0 and 1 atomic layer, followed by a sharp rise from 1 to 5 atomic layers, which then gradually levels out for incident energies $\leq$ 500 ev., becoming horizontal at about 15 atomic layers at 500 ev. incident energy. For higher primary energies, the sharp rise from 1 to 5 atomic layers is

followed by the gradual curving over, but δ does not become constant; instead it shows a much more gradual, linear rise as the film thickness is increased from about 15 to 35 atomic layers, the latter value being the thickest film measured.

It is possible to explain this behaviour in terms of the reflected electrons. The reflection coefficient r of platinum (Z = 78) is considerably greater than that of aluminium (Z = 13) even at primary energies as low as 1 kev. (Sternglass, 1954). The linear rise in δ as the platinum film thickness increases beyond 15 atomic layers is probably due to an increase in reflected electrons, and the secondaries they generate near the surface as they leave the material. Since r increases with primary energy in the 1 to 5 kev. range, this explanation suggests that the observed slope of δ vs. thickness of the evaporated layer should be greater for 3 kev. primary energy than for 1 kev. primary energy in the linear region of the curve (thickness greater than 15 atomic layers). Copeland's experiments (1940, Fig. 3) confirm this. It is therefore reasonable to surmise from Copeland's work that the maximum depth of platinum from which a secondary escapes is from 10 to 15 atomic layers, or 40 to 60 A, from the surface. The mean depth of origin is less.

The above conclusion favours Sternglass and Wachtel's measurements of L, rather than Becker's.

5.5. The Influence of the Reflected Electrons on δ_s.

As the reflected electrons leave the target, they can excite secondary electrons. In fact, since n(x) increases as the exciting electrons' energy decreases, more secondary electrons should be excited as an electron leaves the target after reflection than as it enters. If the target atomic number Z lies between 30 and 80, from 0.3 to 0.5 of the primary electrons are reflected at the voltages of interest, (5 to 30 kv), and a large fraction of the secondary electrons are probably excited by reflected electrons, not primary electrons. Bruining (1954, p. 48) reports that Wecker has measured both the transmitted current and the secondary electron current on the exit side of a thin aluminium foil bombarded with primary electrons of energy 10 to 80 kev. This experiment showed that the number of exit-side secondaries was maximum when about one-half the primary beam was transmitted, but the ratio of secondary current to transmitted current was largest when only a very small fraction of the primary beam was transmitted; i. e., as the average energy of the transmitted electrons increased, the number of secondaries produced per transmitted electron decreased. Since a reflected electron leaving a surface would behave much as a transmitted electron leaving a thin foil, this measurement indicates that reflected electrons will excite secondaries, the number of secondaries excited per reflected electron decreasing as the reflected electron energy increases. It is not

surprising that the experimental universal curve of δ vs. E_o shows an increasing divergence from the theoretical curve as E_o increases above $E_{o_{max}}$.

5.6. The Area of Exit of the Secondary Electrons.

In considering the area from which the secondary electrons leave the specimen, which shall be taken to be a plane smooth surface for the present, the secondaries are conveniently divided into two groups: (1) secondaries excited by the primary beam as it enters the specimen, and (2) secondaries excited by the reflected electrons leaving the specimen.

5.6.1. Exit Area of Primary Beam Excited Secondaries.

This has been worked out by Wells (1957, p. 108) who found that for an infinitely narrow beam at normal incidence, one-half of the secondary current was emitted inside a circle of diameter 0.8 L. A greater fraction will be emitted inside a circle of diameter L. If d_o is the diameter of the incident beam, the exit diameter may be found by the formula

$$d = \sqrt{d_o^2 + L^2} \tag{8}$$

For platinum, $L \leq 50$ A., and if d_o is also reduced to this value, d is about 70 A., which gives a rough indication of the smallest area from which the secondary electrons excited by the primary beam may emerge.

5.6.2. Exit Area of Reflected Electron Excited Secondaries.

The secondaries excited by the reflected electrons will emerge over approximately the same area as the reflected electrons. While the upper limit of this area is a circle of radius R = range, there is no easy way to calculate the intensity distribution of reflected electrons in this circle. Densitometer studies on negatives of p-n junctions show that most of the change in density for a straight junction in the plane of the beam axis and the specimen normal takes place in a distance of 0.5 (±0.2) micron. Since the calculated range for this specimen at the pertinent voltage is 1 micron, this measurement indicates that the exit area may be approximated by a circle of radius R/4 (or for oblique incidence, an ellipse with minor axis R/4).

It is important to realize that secondary electrons emerging outside of the area of the picture element do not contribute information about that element in a high resolution picture. If two adjacent picture points are to be resolved, the difference in the number of secondaries omitted by each must be large enough to show a contrast greater than the threshold contrast, C_t; symbolically, if N_1 and N_2 are the number of electrons from the picture elements, $N_1 \geq N_2$,

$$C = \frac{N_1 - N_2}{N_1} . \qquad (9)$$

Previously N_1 and N_2 have been taken as all secondary electrons emitted by the specimen when the primary beam strikes picture

elements 1 and 2 respectively. For low resolution pictures there is no difference in the old and new expressions; for high resolution pictures, the difference may become appreciable.

5.7. Specimen Contrast in Terms of Secondary Emission.

Smith (1956) and Wells (1957) have discussed this point. Smith merely pointed out that the number of secondary electrons would change with incident angle. Wells quoted data from the literature to show that the increase in secondary emission follows roughly a $\sec\beta$ law, where β is the angle between the specimen normal and the incident beam. It was shown in Section 2.7.6. that the secondary electrons which are collected from a smooth specimen do vary as $\sec\beta$. If δ_β is the value of δ at β, and δ_o is the value at $\beta = 0$, then

$$\delta_\beta = \delta_o \sec\beta , \tag{10}$$

$$\Delta\delta_\beta = \delta_o \sec\beta \tan\beta \, \Delta\beta \tag{11}$$

and

$$C = \frac{\Delta\delta_\beta}{\delta_\beta} = \tan\beta \, \Delta\beta \tag{12}$$

This expression allows the minimum angular variation between two picture elements to be written as

$$\Delta\beta_{min} = C_t \cot\beta \quad \text{radian}, \tag{13}$$

where β is the larger value of angle subtended between the element normals and the incident beam. $\Delta\beta_{min}$ decreases as β increases; i.e., better contrast is obtained at larger values of β, as well as greater brightness.

If $\beta = 65^{\circ}$, and $C_t = 0.05$, then the minimum detectable change in specimen angle is about 1.3°. This is about twice the minimum detectable change calculated in Section 4.3. from McMullan's data. It follows that for $\beta = 65^{\circ}$, the contrast observed on a reflected electron micrograph should be about twice that observed on a secondary electron micrograph, and indeed, considerably more contrast is observed on the reflected electron micrographs of Figs. 2.4. and 2.5., Section 2.3., than on the secondary electron micrographs.

The above remarks are valid for a surface with only small angular variations. If the specimen surface is rough, two additional effects must be considered: surface modulation and specimen collection of the escaping secondary electrons. Sections of a rough specimen are schematically represented in Figs. 5.2. and 5.3. In these two dimensional figures, the specimen normal is in the plane of the paper, but the primary beam may make an angle β with this plane. The estimated intensity distributions are shown in Fig. 5.2. for three cases of surface modulation: (A) plane surface, (C) sharp peak, and (B) sharp valley. These three cases represent normal area of escape, greater area of escape, and smaller area of escape for the secondary

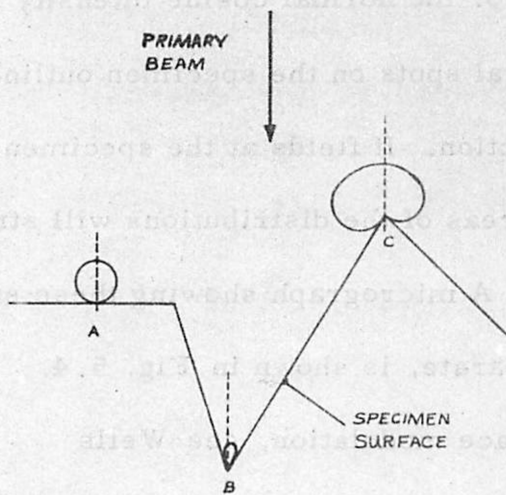

Fig. 5.2. Diagram illustrating surface modulation as discussed in text.

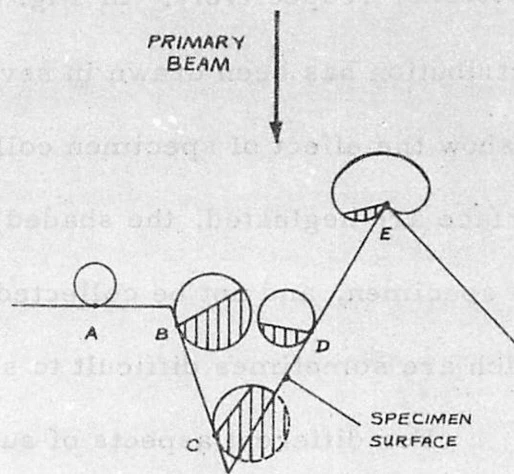

Fig. 5.3. Diagram illustrating specimen collection as discussed in text.

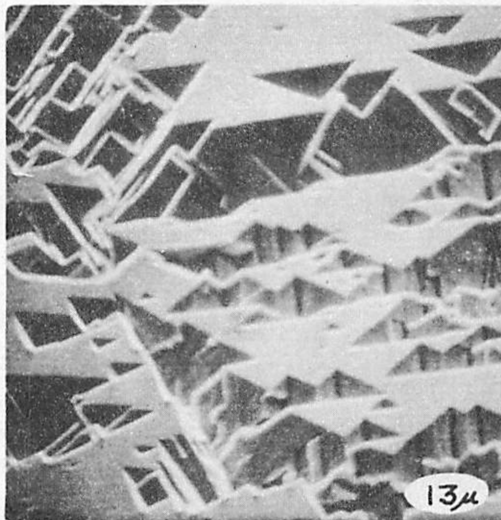

Fig. 5.4. Micrograph of Etched Aluminium illustrating surface modulation and specimen collection.

electrons, respectively. In Fig. 5.3. the normal cosine intensity distribution has been drawn in several spots on the specimen outline, to show the effect of specimen collection. If fields at the specimen surface are neglected, the shaded areas of the distributions will strike the specimen, and not be collected. A micrograph showing these effects, which are sometimes difficult to separate, is shown in Fig. 5.4.

For different aspects of surface modulation, see Wells (1957, Chapter 8).

CHAPTER 6.

NOISE LIMITATIONS.

In any physical system fluctuation phenomena impose a lower limit to the contrast which can be observed. This is why the threshold contrast of the eye increases as the brightness decreases below a few foot lamberts. Noise limits, and threshold contrast, have been discussed in general terms by Rose (1948) and Zworykin and Morton (1954). McMullan (1952) and Smith and Oatley (1955) have discussed noise in the scanning electron microscope, assuming that the electron current fluctuations are always random, and that the noise is determined at the point where the mean electron current is minimum. A more general theory, including the noise generated by secondary emission, is presented here; this theory follows directly from the work of Shockley and Pierce (1938). Similar theories about the noise of secondary emission may be found in van der Ziel (1955) and Zworykin and Morton (1954).

6.1. Theory.

For the present, assume all electrons coming from the specimen are collected. Let n be the number of primary electrons striking each

picture element on the specimen surface, $\bar{n}$ be the average value of n, and $\overline{(n - \bar{n})^2}$ be the mean square deviation of n. Let each primary electron have a probability $p(\delta)$ of producing δ secondary electrons. If N is the number of secondary electrons produced by n, $\bar{N}$ the average value of N, and $\overline{(N - \bar{N})^2}$ the mean square deviation of N, it immediately follows that

$$\bar{N} = \bar{\delta}\,\bar{n} \,. \tag{1}$$

A formula for the mean square deviation of N has been derived by Shockley and Pierce (1938, p. 323), and written in the above notation, is stated here without proof.

$$\overline{(N - \bar{N})^2} = \bar{\delta}^2\, \overline{(n - \bar{n})^2} + \bar{n}\, \overline{(\delta - \bar{\delta})^2} \tag{2}$$

This formula can be simplified by assuming that the primary electrons are described by a random distribution, such as a Poisson distribution. Mathematically, this means that

$$\overline{(n - \bar{n})^2} = \bar{n} \tag{3}$$

and therefore

$$\overline{(N - \bar{N})^2} = \bar{\delta}^2\, \bar{n} + \bar{n}\, \overline{(\delta - \bar{\delta})^2} \tag{4}$$

Before proceeding further, it is convenient to relate the above quantities to contrast. If all N of the electrons coming from a picture element contribute equally to the video signal, N may be taken as the

equivalent brightness of that picture element, and contrast may be written as

$$C = \frac{\Delta N}{N} . \tag{5}$$

The minimum detectable contrast or threshold contrast at the specimen may be related to the root mean square deviation of N by

$$C_t = k \frac{\sqrt{\overline{(N - \overline{N})^2}}}{\overline{N}} , \tag{6}$$

where k is called the threshold signal-to-noise ratio after Rose (1948) and is related to the probability of detection of a given contrast between two picture elements. Substituting equations (1) and (4) into (6),

$$C_t = \frac{k}{\sqrt{n}} \left\{ 1 + \frac{\overline{(\delta - \overline{\delta})^2}}{\overline{\delta}^2} \right\}^{\frac{1}{2}} . \tag{7}$$

Shockley and Pierce have designated the second term in the brackets, the relative mean square deviation of δ, as b. Following their lead,

$$C_t = \frac{k}{\sqrt{n}} (1 + b)^{\frac{1}{2}} . \tag{7a}$$

Assuming perfect collection, and $\overline{\delta} \geq 1$, this expression for threshold contrast is larger than the ones used previously by the factor $(1 + b)^{1/2}$.

A clearer idea of the values b may assume in theory and in practice is given in the following sections.

6.2. Discussion of b.

If δ varies in a random manner about $\bar{\delta}$, $p(\delta)$ can be represented by a Poisson distribution. In this case, $b = 1/\bar{\delta}$ and b is minimum when $\bar{\delta}$ is maximum.

Kurrelmeyer and Hayner (1937) studied the fluctuations in secondary emission for beryllium and nickel at normal incidence; b has been calculated from their published data, and is plotted in Fig. 6.1., together with $\bar{\delta}$ and $1/\bar{\delta}$ for beryllium. (The high value of $\bar{\delta}$ which they observed suggests that their material was beryllium oxide, not beryllium.) Observe that for beryllium, the maximum value of $\bar{\delta}$ occurs at 600 volts, while the minimum value of b occurs at 250 volts; the corresponding values for nickel are 900 volts and 350 volts respectively. Observe also that b increasingly departs from the $1/\bar{\delta}$ curve for $V > 250$ volts. For these materials, and primary voltages greater than about 250 volts, $p(\delta)$ must depart from a random (Poisson) distribution. It may be mentioned in passing that secondary electron multipliers are generally designed to work at 100 to 200 volts per dynode, a voltage range where b is small.

Fig. 6.2. demonstrates that b increases above the value predicted by a random distribution of δ about $\bar{\delta}$ as an approximately

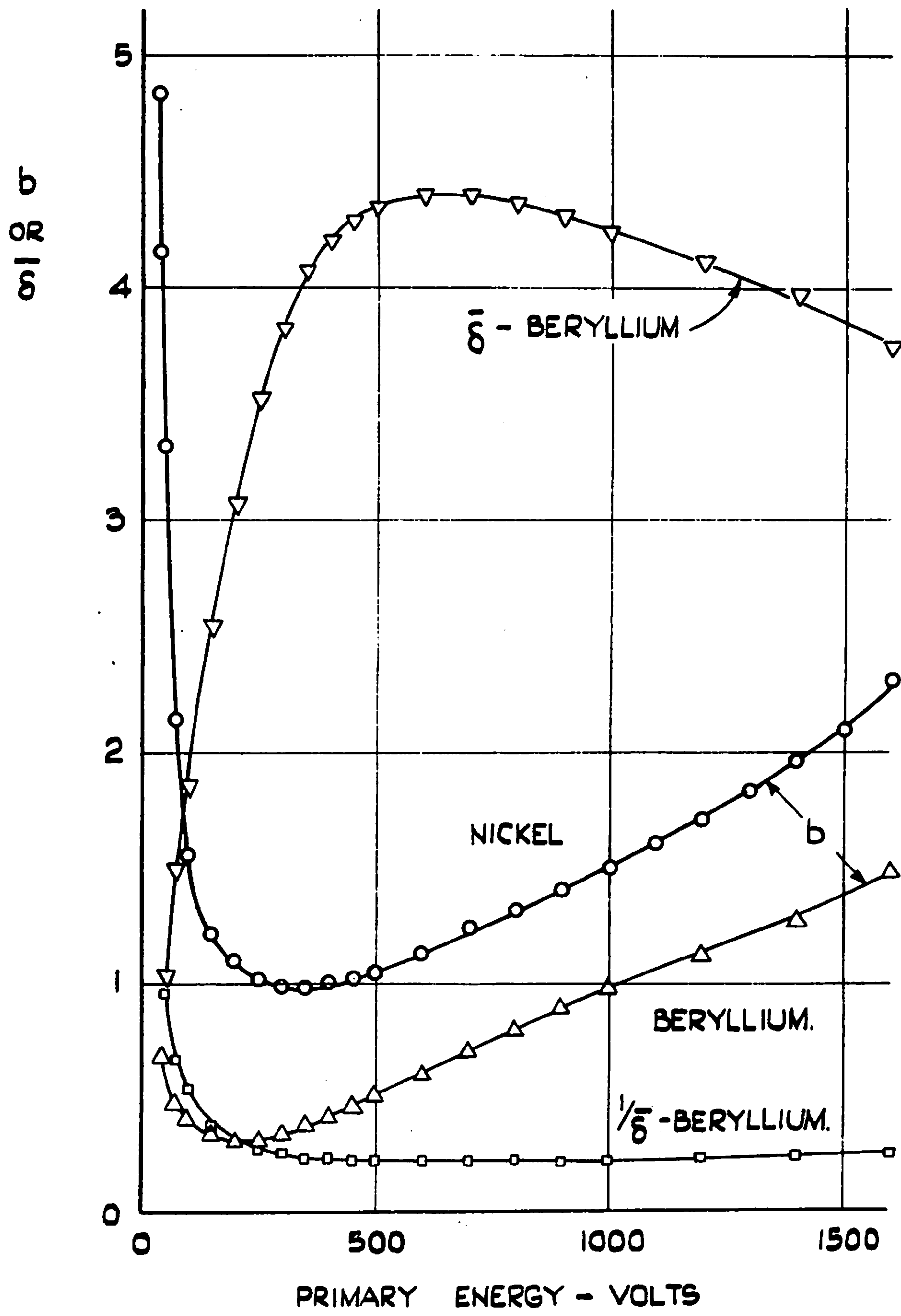

FIG 6.1.

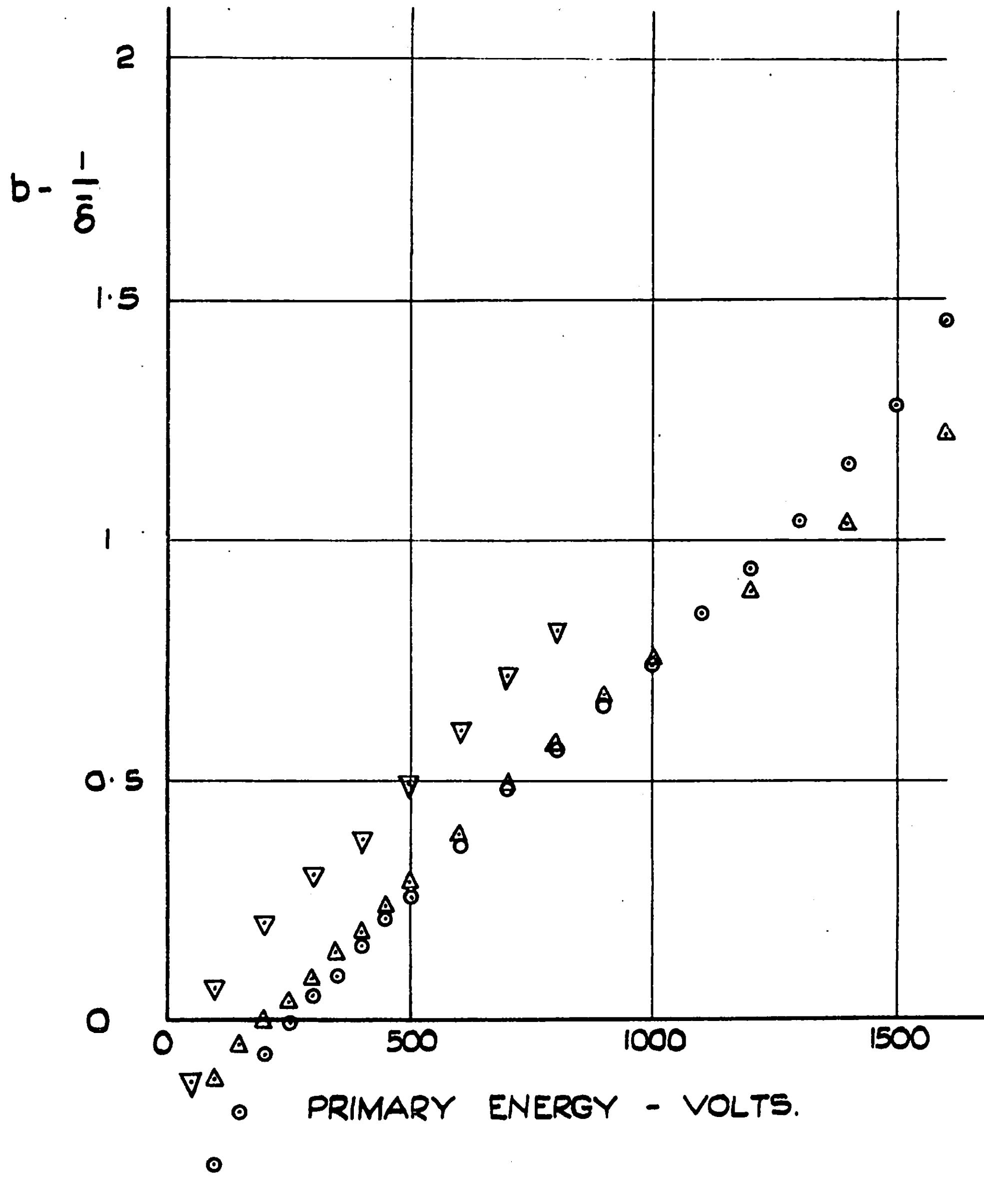

FIG. 6.2.

linear function of primary energy, to the maximum energy measured, 1600 volts. Data at higher energies is unfortunately not available. Measurements of b as a function of primary beam energy and angle of incidence would be of great interest; lacking such measurements, it is necessary to extrapolate the known curves to estimate what value b has at the primary voltages of interest in scanning electron microscopy. If the slope of Fig. 6.2. remains constant to 15 kv., b would be approximately equal to 15 at that voltage. It seems reasonable to suppose, on the information available, that at a primary voltage of 15 kv., b will lie between 10 and 20, say. Before discussing the implications of this value of b to the scanning microscope, it is worthwhile to point out possible reasons for this large increase in b.

Kurrelmeyer and Hayner assumed that many high energy electrons are buried in the target without producing any secondaries, and this reduction in the effective primary beam causes the increase in b. It is also possible that the reflected electrons contribute directly and indirectly to the increase in b. This may be seen as follows: assume that $\overline{\delta}$ is 0.5, $\overline{\delta}_s$ is 0.4, and $\overline{r}$ is 0.1. The preceding chapters have suggested that some of the secondary electrons are excited by reflected electrons; thus for each reflected primary $\overline{\delta} \geq 1$, while for each non-reflected primary, $\delta \leq 0.4$. This shows a large spread in δ, which qualitatively helps explain the increase in b.

On the basis of the above argument, the increase in noise of the secondary electron component, δ_s, should be less than the increase in noise for the total secondary emission, δ, and if the scanning electron microscope image is derived only from secondary electrons, the increase in noise will probably be less than predicted by using the value of b found by Kurrelmeyer and Hayner.

6.3. Noise Limitations in the Scanning Electron Microscope.

If a 5% contrast between two picture elements is to be detected with reasonable certainty on a micrograph, the threshold contrast, C_t, must be less than 5%. $\bar{n}$ can be written in terms of the primary beam current I, the number of picture elements per micrograph, P, the time necessary to record one micrograph, T_s, and the electronic charge e:

$$\bar{n} = \frac{I\,T_s}{e\,P} \quad . \tag{8}$$

If (8) is substituted into (7a), C_t is obtained in terms of these parameters

$$C_t = k\left\{\frac{e\,P(1+b)}{I\,T_s}\right\}^{\frac{1}{2}} \tag{9}$$

For small values of C_t, I and T_s should be large, and P should be small.

Langmuir (1937) has shown that for a given current density at the cathode j_o, at an absolute temperature $T^oK.$, the maximum current density which can be obtained depends only on the angular aperture α and the accelerating voltage V. Smith (1956) showed that if the gaussian diameter of the final spot, d_g, contains by definition 80% of the beam current, the primary beam current at the specimen is given by the modified Langmuir equation

$$I = 0.62 \, j_o \cdot \frac{e \, V}{k \, T} \, \alpha^2 \cdot \frac{\pi \, d_g^2}{4} \quad . \tag{10}$$

V and α must be large for large currents in a given spot diameter.

If α is large, spherical aberration and astigmatism impose a lower limit on the spot diameter (see Smith, 1956, Section 2.2.3.). The latter fault can be corrected with a stigmator, so the discussion here will be confined to the former. The diameter of the disk of confusion due to spherical aberration is written by Zworykin et al. (1945) as

$$d_s = 0.4 \, C \, f \, \alpha^3 \, . \tag{11}$$

Following McMullan (1953), to obtain the maximum current in a gaussian spot of diameter d_g, α should be increased until $d_s = d_g$. Since α is then known in terms of d_g, α can be eliminated from equation (10), giving

$$I = 0.62\ j_o \cdot \frac{e\ V}{k\ T} \cdot \frac{\pi}{4} \cdot \frac{d_{gs}^{8/3}}{(0.4Cf)^{2/3}} \tag{12}$$

where d_{gs} is written to indicate $d_g = d_s$. The diameter of the final spot d can be found if the current density across the disk of confusion has a gaussian distribution; in this case,

$$d = \left\{ d_g^2 + d_s^2 \right\}^{\frac{1}{2}} = 1.4\ d_{gs} \quad . \tag{13}$$

Using equations (9) and (12), C_t may be written as

$$C_t = 5.32 \cdot 10^{-12}\ k \left\{ \frac{P(1+b)}{T_s} \ \frac{T}{j_o\ V} \right\}^{\frac{1}{2}} (CF)^{\frac{1}{3}}\ d_{gs}^{-\frac{4}{3}} . \tag{14}$$

This equation shows the variation of threshold contrast with parameters of interest in the design of scanning electron microscopes, when only spherical aberration limits the current in the final spot. Under these conditions, for a given value of d_{gs}, and assumed values of all parameters except the recording time, T_s, the latter can be calculated for the desired value of threshold contrast. Equation (14) can also be used to calculate the value of threshold contrast which might be expected on a high resolution micrograph. Suppose for example that the gaussian spot and the disk of confusion resulting from spherical aberration are both reduced to a diameter of 70 A. The final spot diameter d is then

about 100 A. Practical limits of filament temperature and current density are $3000^{\circ}K$ and 10 amp/cm^2. The recording time has an upper practical limit of about 5 minutes, and the minimum useful number of picture elements per micrograph is rather arbitrarily set at 10^5. (Smith and Oatley (1955) quote 10^6 as a reasonable number for a useful field of view). Cf is about 10 cm for the electrostatic lens now used, and b is estimated to be about 15 at the typical operating voltage of 15 kv. Rose (1948) takes $k = 5$. Substituting all these numbers into equation (14), the value of threshold contrast at a final spot diameter of 100 A is found to be about 0.1. Micrographs with this threshold contrast would yield much useful information; even under the more stringent noise considerations of this chapter, resolutions of under 100 A should be within reach with the scanning microscope.

If the primary current at the specimen is known, equation (9) can be used to calculate the threshold contrast. For the present instrument, $P = 1.6 \times 10^5$, $T_s = 200$ sec., $I = 20 \times 10^{-12}$ amp and using $b = 15$, $V = 15$ kv., and $k = 5$, C_t is found to be about 0.05; i.e., the present micrographs should be just noise free.

It should be mentioned that if b is a linear function of voltage as an extrapolation of Fig. 8.2. would indicate, then for $b >> 1$, the threshold contrast as given by (14) is practically independent of voltage.

PHOTOGRAPHIC NEGATIVE DENSITY VS. C.R.T. BIAS POTENTIAL

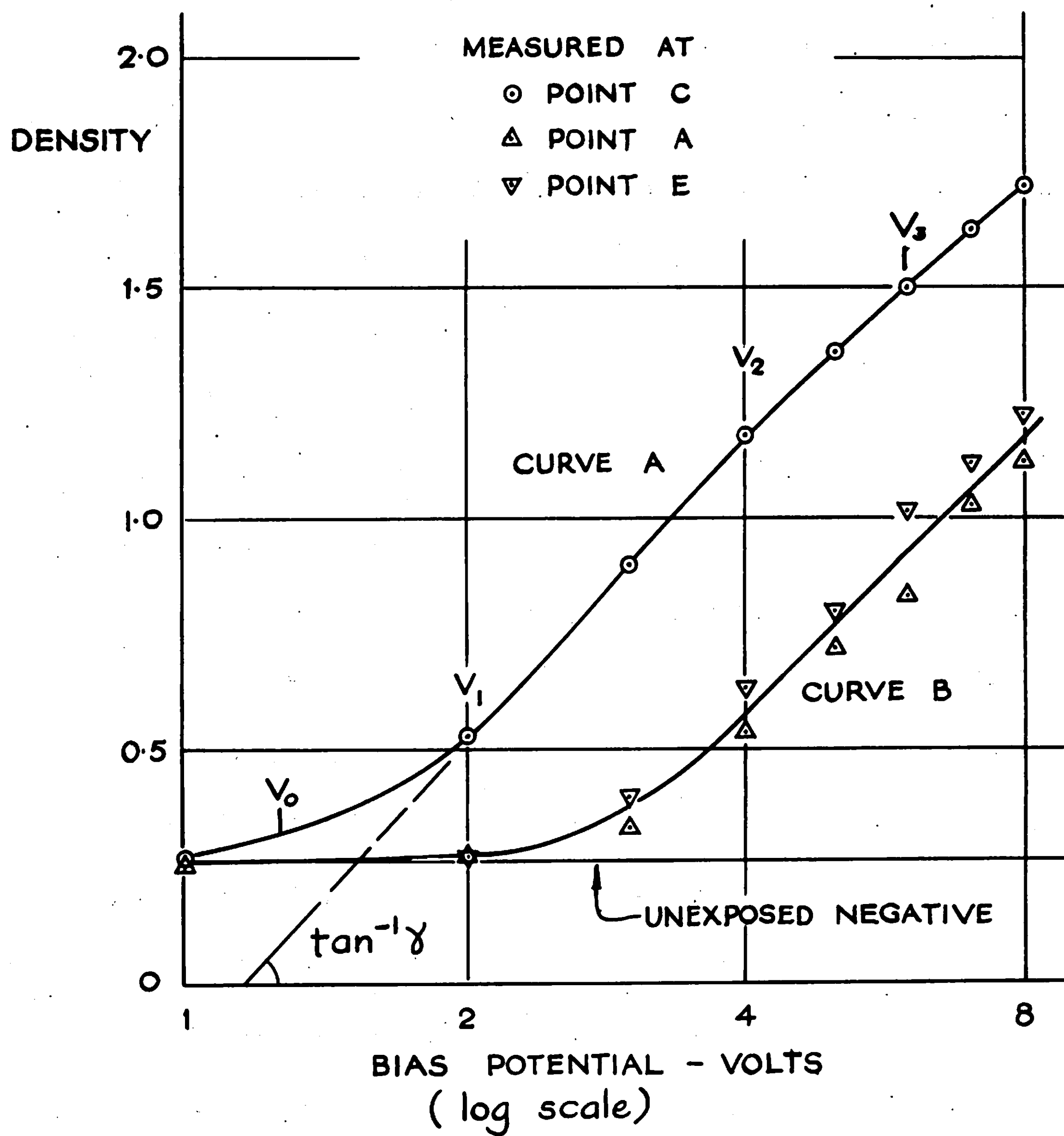

FIG. 8.2.

6.4. Collection Noise.

In the above sections, it has been assumed that all secondary electrons are collected and contribute equally to the video signal. In Chapter 2 it was reported that the current striking the scintillator was greater than the current leaving the specimen, indicating that there was some electron multiplication between the specimen and scintillator. This is almost certainly due to the shape of the collector shield around the scintillator, and since b is small for the energies with which a secondary electron from the specimen will strike this shield (100 to 200 volts) this multiplication is nearly noise free. Since each electron striking the scintillator produces about 50 photons, little noise will be introduced here. The number of electrons produced at the photocathode is about twice the number striking the scintillator, and while strictly speaking the noise introduced at this stage should be included in the analysis, in practice photomultipliers are relatively free of noise, and this omission seems justifiable.

On the basis of the results quoted in Chapters 2 and 7 it is believed that almost all of the secondary electrons are collected and recorded; collection noise therefore may legitimately be neglected.

CHAPTER 7.

COLLECTION CONTRAST

If two picture elements on the specimen surface, A and B, emit the same number of secondary electrons, but more are collected from A than from B, collection contrast will be observed on the micrograph. In the more general case, when the number of secondary electrons emitted by A and B differ, if the fraction collected from A is larger than the fraction collected from B, collection contrast is superimposed on specimen contrast, and either more or less contrast will be observed than would be predicted from the preceding Chapters.

7.1. Specimen Collection.

One obvious example of collection contrast is specimen collection, which was discussed in Section 5.7. Fig. 7.1. shows a germanium specimen with a series of holes on its surface probably produced by strains. Secondary electrons produced in these holes have little chance of escaping and reaching the collector, and so the holes appear black on the micrograph.

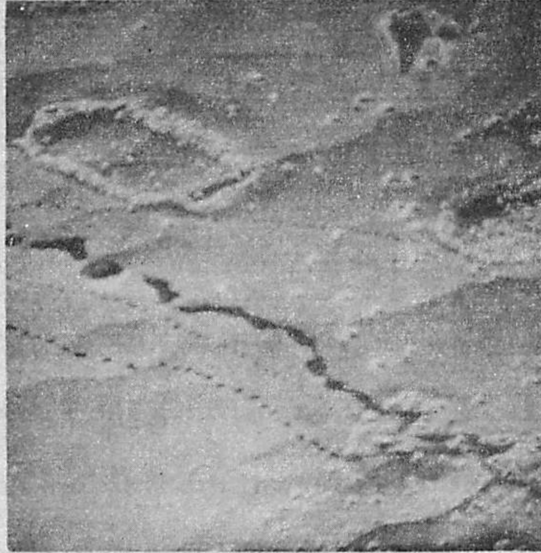

Fig. 7.1. Micrograph of germanium surface illustrating specimen collection. M = 650.

7.2. Specimen-Collector Electron Trajectories.

The electron trajectories in the specimen chamber must be known before any accurate estimate of collection efficiency or collection contrast is possible. Because the complicated electrode configuration in the specimen chamber makes calculation extremely difficult, the trajectories shown in Chapter 2 and this chapter were plotted in the laboratory automatic electron trajectory tracer (see Pizer, Yates, and Sander, 1956) with the cooperation of M. R. Barber. All plotted trajectories lie in the plane of symmetry of the specimen chamber, which is defined by the beam axis and the specimen normal. If initial electron velocities and specimen-collector transit times are known, trajectories outside this plane may also be estimated. McKay (1948, Table II, p. 83) has reported that for many materials the most probable secondary electron energy is between 2 and 6 volts; therefore an initial energy of 4 volts has been taken as a standard value for these traces, except when initial energy has been the parameter.

Trajectories of 4 volt electrons emitted at different angles and different positions on the specimen are shown in Fig. 7.2. Note that some electrons strike the final lens, and therefore do not contribute to the video signal. By increasing the collector potential to the more usual value of 200 volts, as shown in Fig. 7.3., final lens collection of 4 volt electrons is reduced to negligible proportions, and it seems probable that even when secondary electrons of all energies are considered final lens collection will be a minor source of contrast.

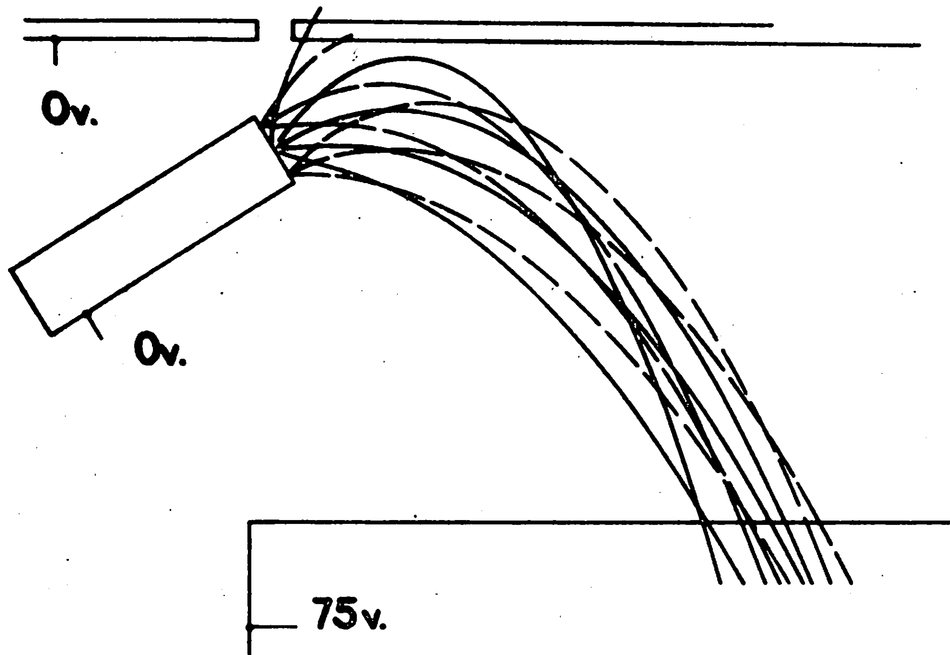

FIG. 7.2. FOUR VOLT ELECTRON TRAJECTORIES EXIT POSITION AND ANGLE VARIED.

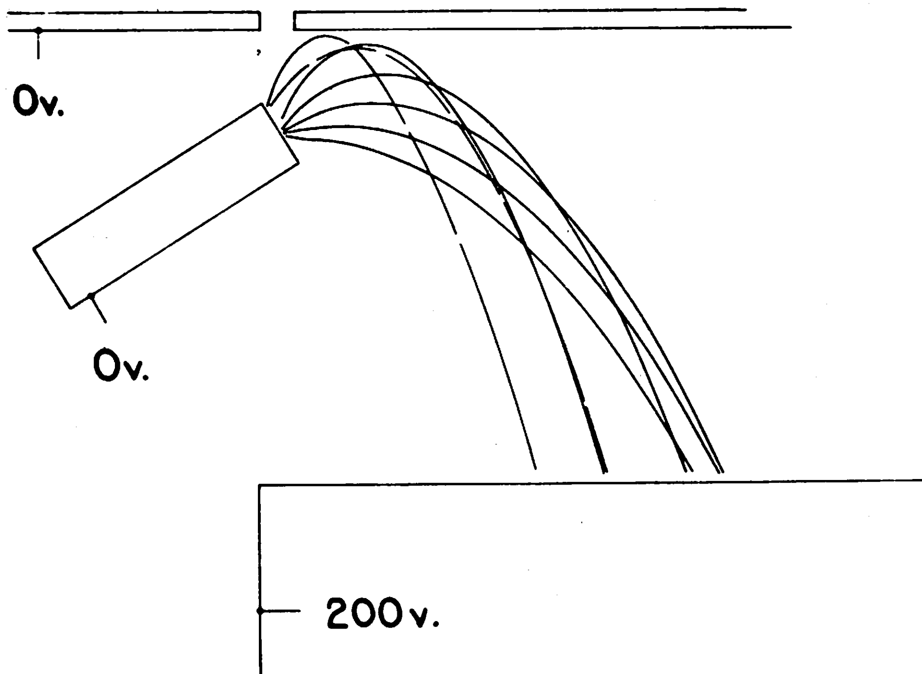

FIG. 7.3. FOUR VOLT ELECTRON TRAJECTORIES EXIT POSITION AND ANGLE VARIED.

Fig. 7.3. shows that for maximum collection efficiency at a collector potential of 200 v, the collector should be positioned about one-eighth of its diameter farther to the right.

Fig. 7.4. shows similar traces for a different collector position. It is evident that as long as the collector is relatively near the front of the specimen, its actual position is not critical for good collection efficiency. Trajectories of electrons emitted along the specimen normal are shown in Fig. 7.5., with initial energy as the parameter; it may be concluded from these two figures that most secondary electrons in the plane of symmetry enter the collector.

Fig. 7.6., coupled with Figs. 7.2. and 7.3., indicate that this conclusion also holds for the usual collector position and voltage.

Fig. 7.7. shows the equipotentials in the specimen chamber. With a collector potential of 200 volts, the field at the centre of a smooth specimen is about 80 volts/cm. The field at sharp discontinuities on the specimen surface (edges of etch pits, for example), may be much higher, and the initial acceleration of the electrons caused by this field will influence the trajectories. An electron emitted in any direction at a sharp point will initially be accelerated in the direction of maximum field intensity, and its trajectory will lie closer to the trajectory of an electron emitted in this direction than would be predicted by the smooth-specimen trajectories plotted here. This effect will probably produce observable contrast only in rare cases.

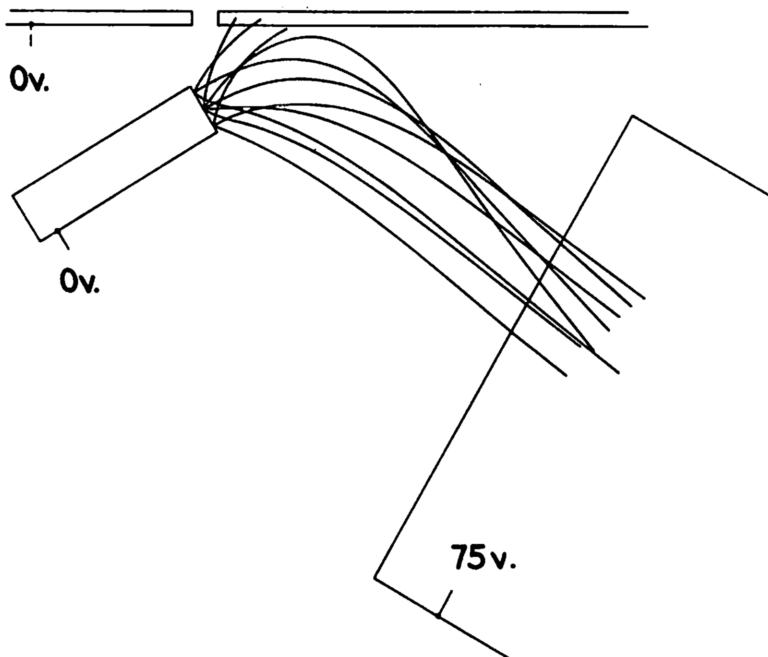

FIG.7.4. FOUR VOLT ELECTRON TRAJECTORIES
EXIT POSITION AND ANGLE VARIED.

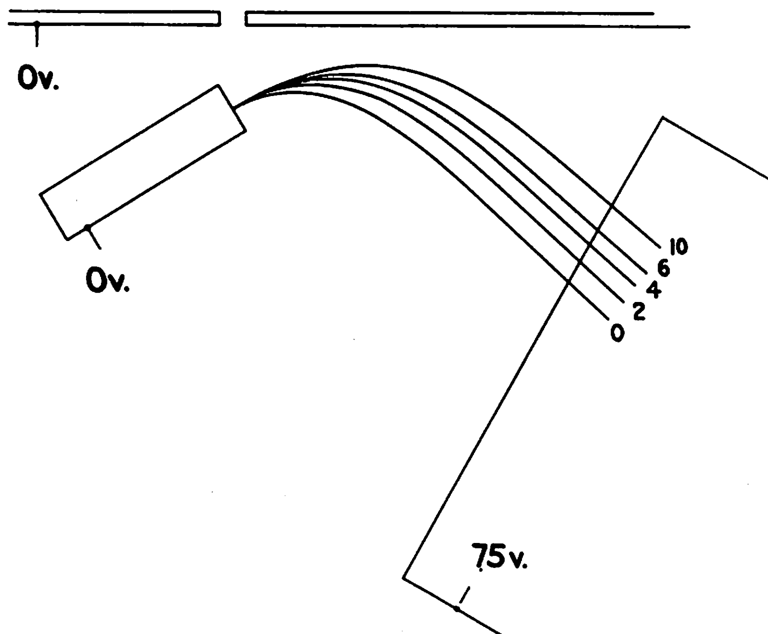

FIG.7.5. VARIABLE ENERGY ELECTRON
TRAJECTORIES.

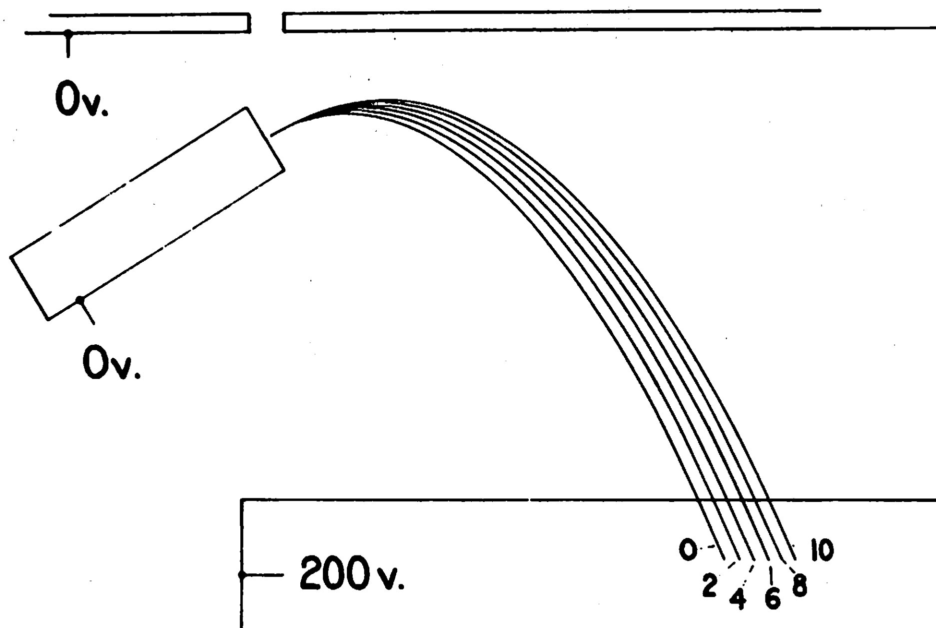

FIG. 7.6. VARIABLE ENERGY ELECTRON TRAJECTORIES.

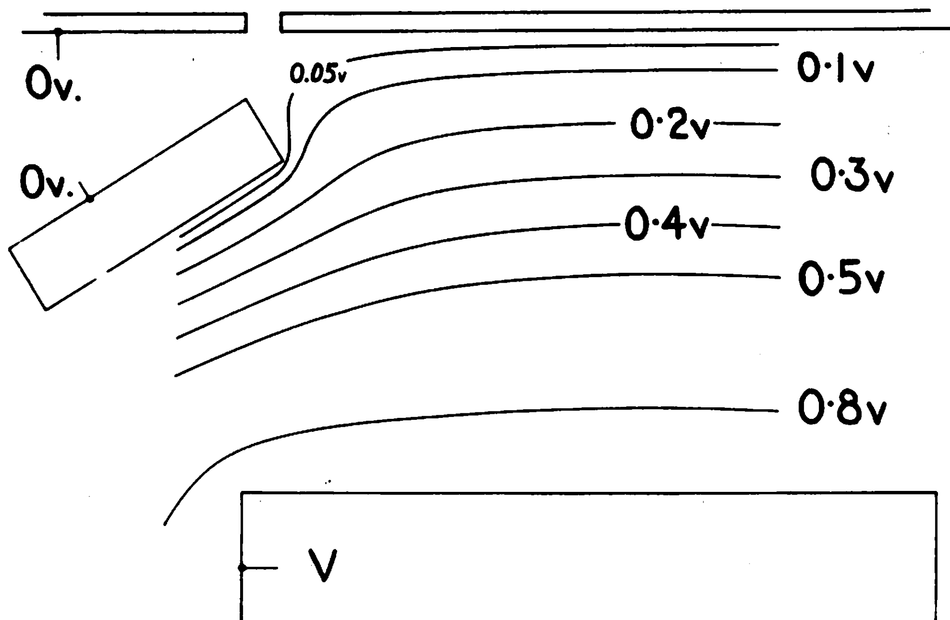

FIG. 7.7. EQUIPOTENTIALS.

7.2.1. Specimen-Collector Electron Trajectories Including the Effect of the Final Lens Potential.

The above trajectories neglect any field from the centre electrode of the final lens, which is normally 15 kv. below earth potential. Fig. 7.8. shows electrons emitted at different angles from the specimen with the lens voltage on and off (solid and dashed lines respectively). Electrode A does not correspond to the centre electrode of the lens, but an equipotential between the centre electrode and the outer electrode, L. The potential and shape of A were found by a relaxation method, utilizing the axial potential as given by Regenstreif (1951, equation 194, p. 46). The potential at the centre of the lens face (point a) was empirically determined in the electrolytic tank to be about - 15 volts. Fig. 7.9. shows a similar trace with the collector held at the more usual potential of 200 volts. It may be concluded from these traces that the leakage field from the electrostatic lens presently used does not appreciably alter the specimen-collector electron trajectories.

The time-pips on the trajectories in Fig. 7.8. show that the mean transit time is about 10^{-8} sec. at a collector potential of 75 volts, and the minimum transit time is about one-half the maximum transit time. This spread in transit times limits the maximum number of picture elements which can be scanned each second to $\sim 5 \times 10^{7}$; this is 100 times the number of picture elements per second currently scanned.

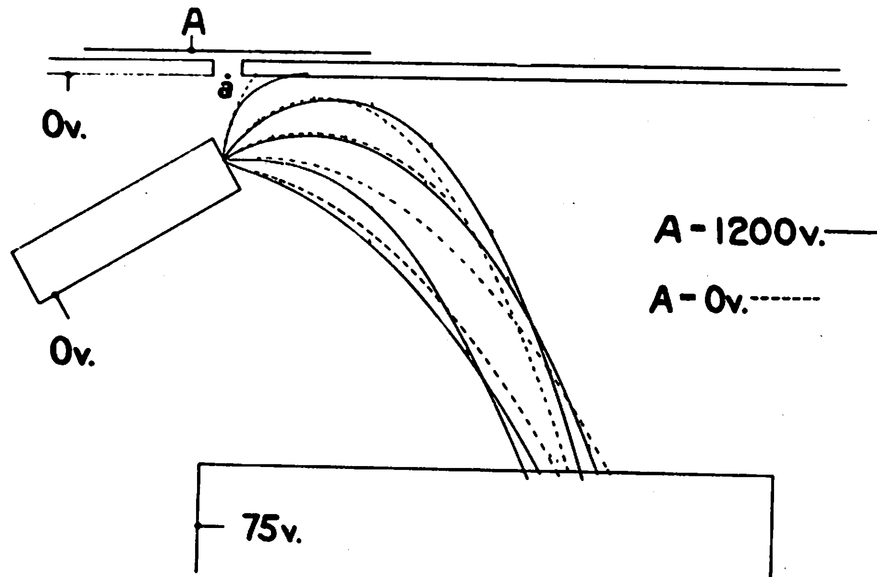

FIG. 7.8. FOUR VOLT ELECTRON TRAJECTORIES INCLUDING FINAL LENS VOLTAGE.

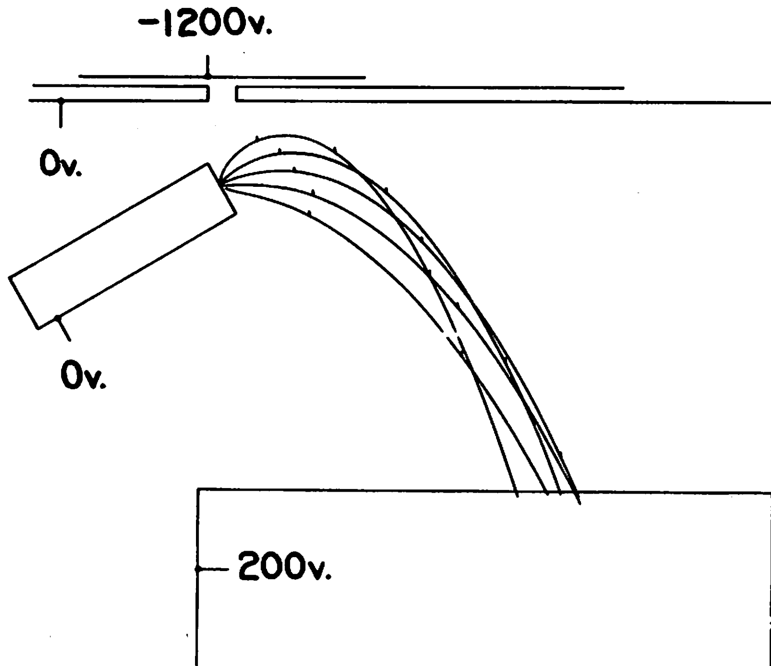

FIG. 7.9. FOUR VOLT ELECTRON TRAJECTORIES INCLUDING FINAL LENS VOLTAGE.

7.3. Voltage Detection.

Smith (1956, p. 125) first observed that the number of collected electrons is a sensitive function of the specimen potential. If the specimen potential varies, the 4 volt electron trajectories shown in Fig. 7.10. are obtained. Similar trajectories with the collector potential set at 200 volts are shown in Fig. 7.11. If all secondary electrons were emitted along the specimen normal, these figures would provide a complete quantitative explanation of voltage detection, i.e., the detection of potential variations on the specimen surface as brightness variations on the CRT display. Because secondary electrons are emitted at all angles with a velocity distribution, these figures only indicate that voltage detection should be possible. By placing a slitted shield over the collector, (slit opening extending from M to N in Fig. 7.10., for example) these figures also indicate that smaller voltages may be detected at the expense of collection efficiency.

While investigations utilizing voltage detection are reported in Chapter 9, one of the first voltage detection micrographs is shown in Fig. 7.12. (same plate as Fig. 7.1.) to illustrate the technique. The specimen is a back-biased junction diode; the dark area on the left was 5 volts positive, the brighter area on the right was at earth potential. The uneven junction is typical of many specimens examined by the author.

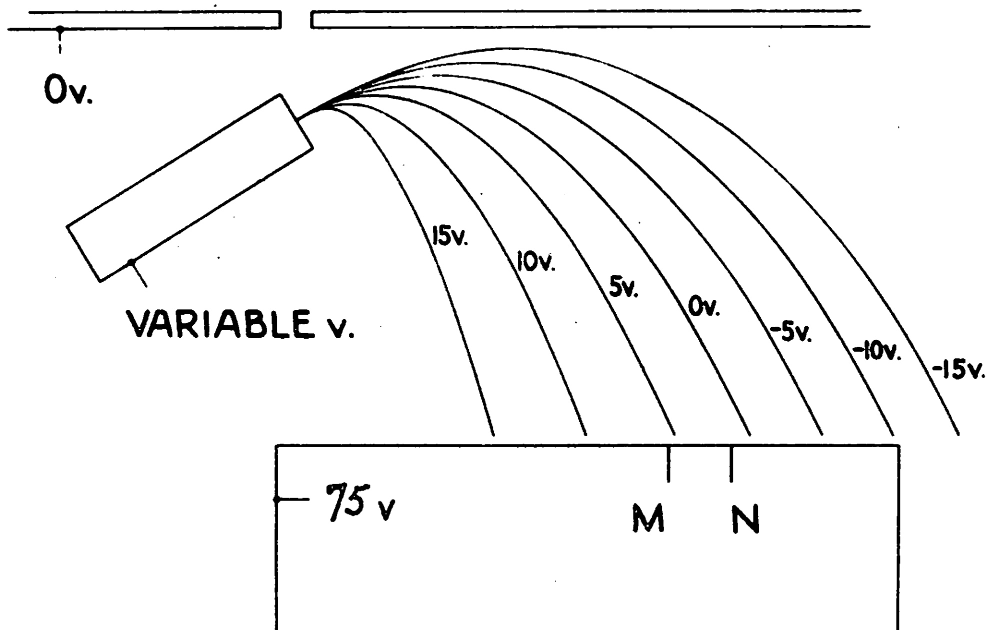

FIG. 7.10. FOUR VOLT ELECTRON TRAJECTORIES SPECIMEN VOLTAGE VARIABLE.

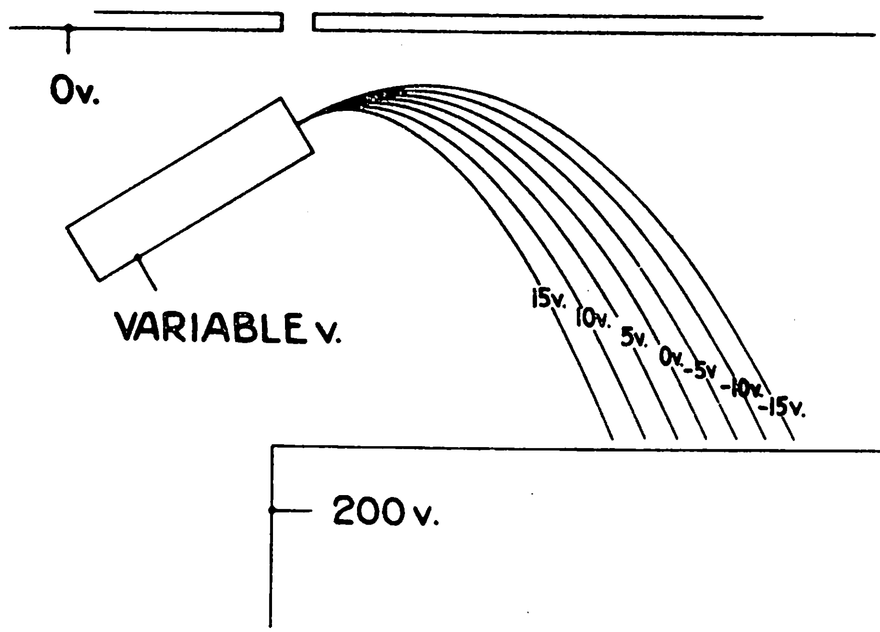

FIG. 7.11. FOUR VOLT ELECTRON TRAJECTORIES SPECIMEN VOLTAGE VARIABLE.

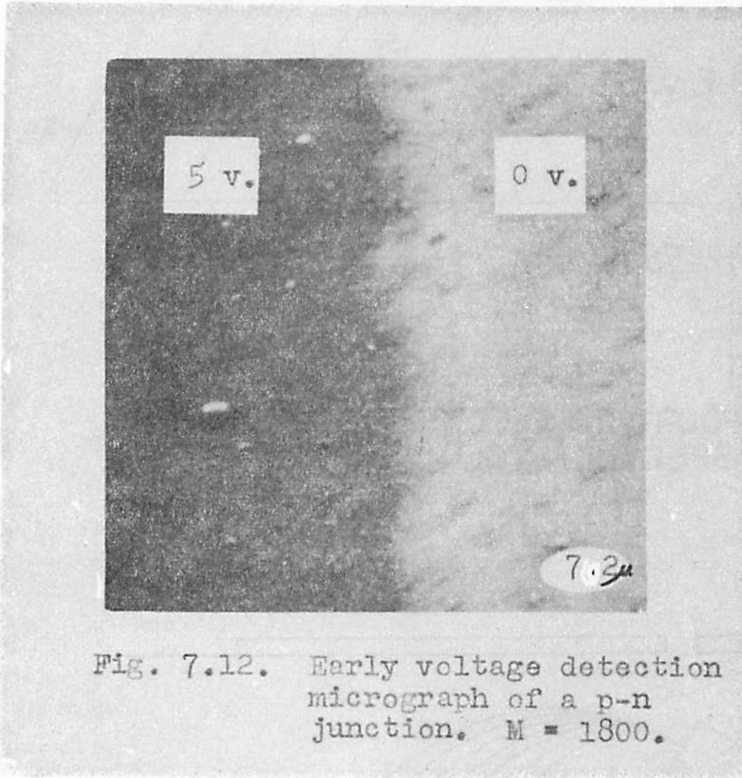

Fig. 7.12. Early voltage detection micrograph of a p-n junction. M = 1800.

The variation of video signal as a function of specimen potential has been studied in the microscope itself, with both the electron multiplier and the scintillator-photomultiplier collection system. The experiments do not include the effects of transverse fields which will exist between two portions of the specimen at different potentials, but they do give a general idea of the contrast which may be expected. Fig. 7.13. shows typical plots of video signal vs. specimen potential.

In certain applications, it is desirable to resolve the smallest possible potential differences. The slope of the curves in Fig. 7.13. at a given specimen voltage, divided by the video output at that voltage, gives the contrast per volt. The smallest detectable potential difference is equal to the threshold contrast, usually taken as 0.05, divided by the contrast per volt, which typically is about 0.1 to 0.15; these values give a minimum detectable potential difference of about 0.5 volt. Using a narrow slit across the electron multiplier input, a contrast per volt of over 1.0 has been measured, which corresponds to a minimum detectable potential difference of about 50 millivolts. The narrow slit greatly reduces the collection efficiency, and to maintain a threshold contrast of 0.05, the beam current (and spot size) had to be increased considerably. While the minimum detectable potential difference observed on micrographs is somewhat lower than the values predicted in the above manner, the agreement is within a factor of two.

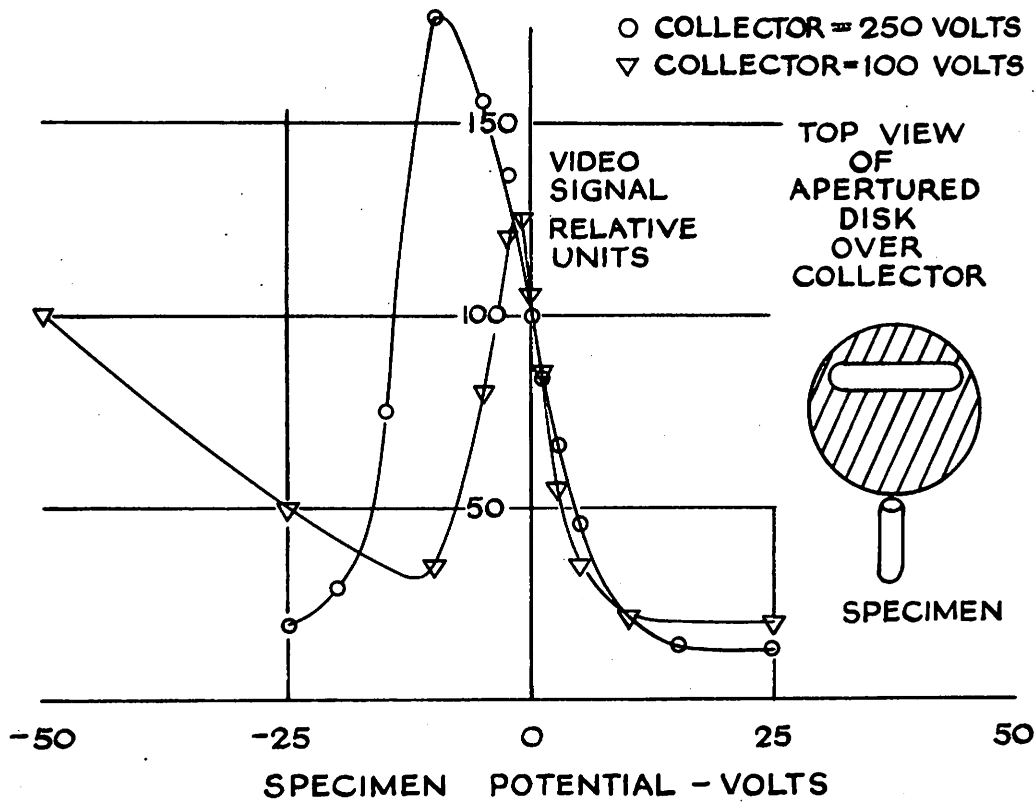

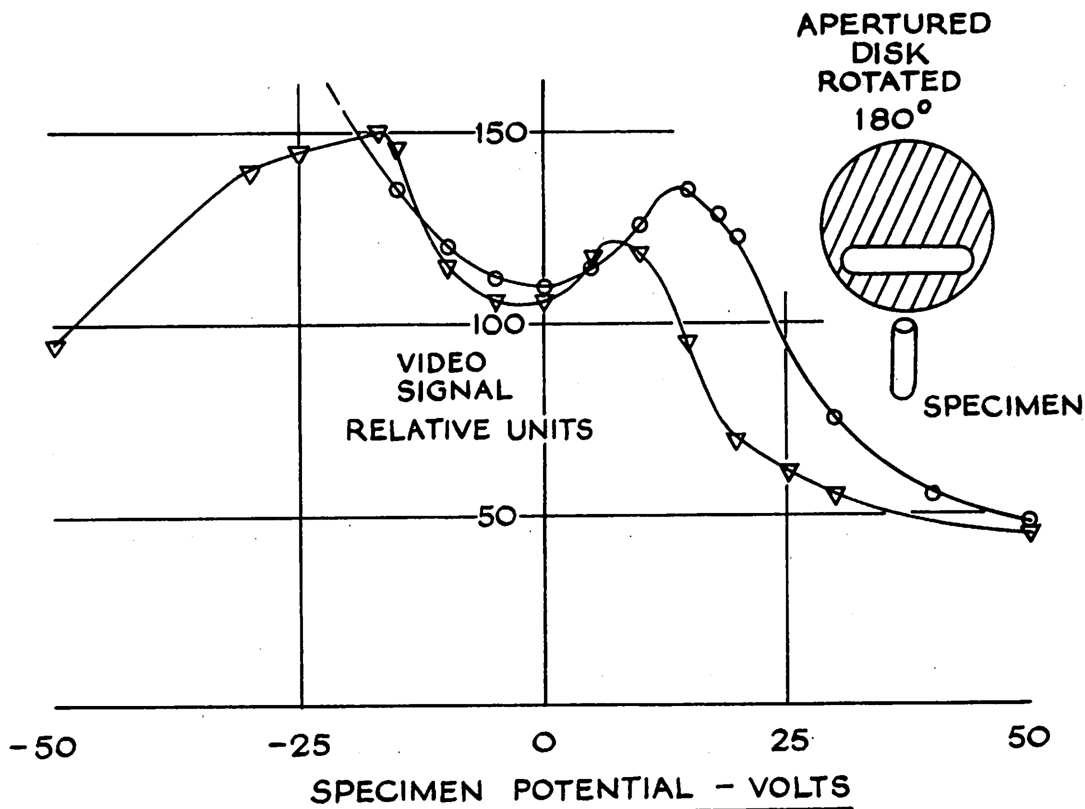

FIG. 7.13.

Fig. 7.13. also provides direct support for the trajectory traces of Figs. 7.2., 7.3., 7.6., 7.10., and 7.11.

7.3.1. The Effects of Transverse Fields.

A transverse field at the specimen surface will accelerate secondary electrons in a direction parallel to the specimen surface. If this direction lies in the plane of symmetry, Figs. 7.14. and 7.15. show typical trajectories. The analogue specimen in this experiment was slit down the centre, to simulate a p-n junction. The field in the gap was 20 V/cm., where V is the potential difference between the two halves of the specimen in volts. Analysis of these and similar traces shows that the angular deflection of four volt electrons caused by the transverse field is about 3.5 V degrees. This deflection will cause appreciable contrast only if the transit time is much longer than at present.

The field in actual junction diodes exists over a much narrower region; typical values are a one volt drop across a region two microns thick, giving a peak field of about 10^4 volts/cm. When the junction plane and the plane of symmetry coincide, secondary electrons may well receive a sufficient deflection from this transverse field to miss the collector completely. It is perhaps significant that the best voltage detection micrographs shown in Chapter 9 have been taken in this configuration with a mean field at the specimen estimated to be only 30 volts/cm., and with the rectangular collector input shown in Fig. 2.1.

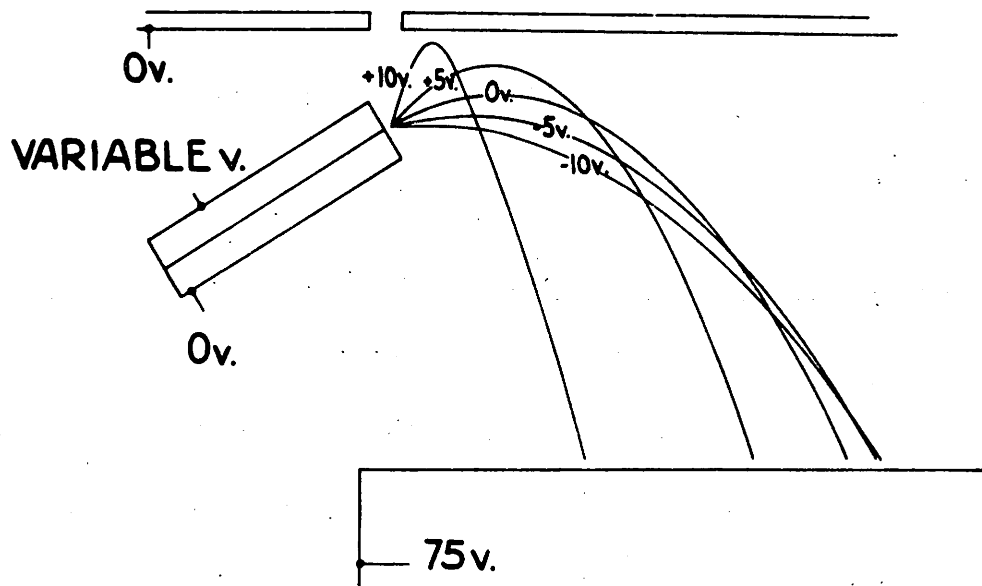

FIG. 7.14. FOUR VOLT ELECTRON TRAJECTORIES SHOWING THE EFFECT OF A TRANSVERSE FIELD AT THE ANALOGUE P-N JUNCTION.

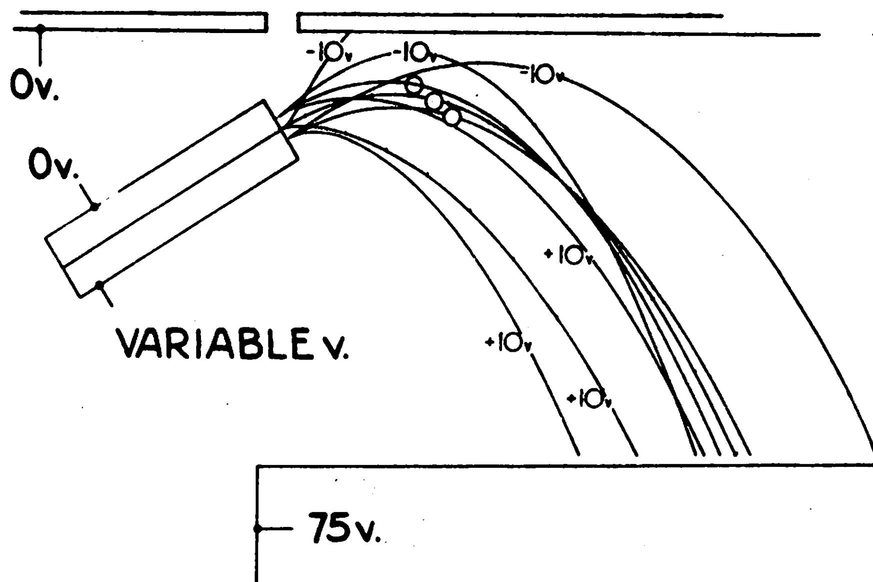

FIG. 7.15. AS FIG. 7.14, EXCEPT THE POTENTIAL OF THE OTHER HALF OF THE ANALOGUE P-N JUNCTION VARIES.

7.3.2. Voltage Detection Using a Grid.

Fig. 2.16. (page 28) shows that voltage detection using a grid near the specimen should give a contrast per volt of 0.15, which is comparable to other methods. Electrons emitted from a positive area of the specimen find themselves in a retarding field, and fewer therefore penetrate the grid and are collected.

7.3.3. Voltage Detection Using a Velocity-Analyser.

A concentric-cylinder velocity-analyser could be used for the most sensitive voltage detection. Electron paths which approximate a circular orbit in such an analyser intersect every 127° (Pierce, 1954, p. 45). The radial position of intersection varies slightly with the electron velocity. If such an analyser were positioned with the cylinder axes perpendicular to the plane of symmetry in the specimen chamber, and if the problem of launching the secondary electrons in the analyser were solved, not only could the electrons be sorted with respect to their velocities normal to the specimen surface, but their velocity spectrum perpendicular to the plane of symmetry (distorted by transverse fields) could also be found. While this system would be very sensitive, considerable effort would probably be required for it to function properly, and it would seem worth investigating only if there is good reason to push voltage detection to its ultimate limit.

CHAPTER 9.

APPLICATIONS OF VOLTAGE DETECTION

If a potential difference exists between two adjacent areas on a smooth specimen surface, under certain conditions a corresponding brightness difference or contrast will be observed on the CRT screen. This contrast is caused mainly by a variation in collection efficiency with specimen potential, as was pointed out in Chapter 7. It occurs because secondary electrons have low energies, and because the specimen-collector field acts as a crude velocity analyser.

9.1. Electrical Characteristics of p-n Junctions.

Before discussing scanning micrographs of p-n junctions, a brief review of their electrical characteristics is desirable. Fig. 9.1. shows the variation of space-charge density, electric field, and potential near an idealized p-n junction. The acceptor density P_o is assumed constant for $x < 0$, and the donor density N_1 is assumed constant for $x > 0$; the graphs have been drawn for the case when $N_1 = 0.1\ P_o$. The electric field E, and therefore the change of potential with distance, is maximum at the junction boundary, $x = 0$, and decreases linearly to zero at the edges of the space-charge region.

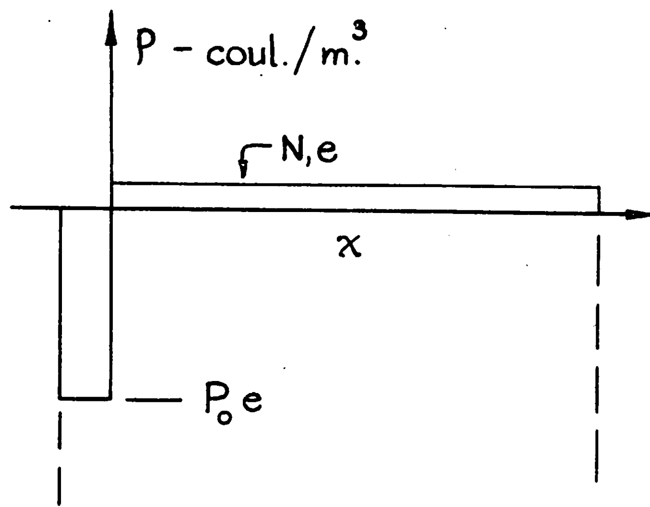

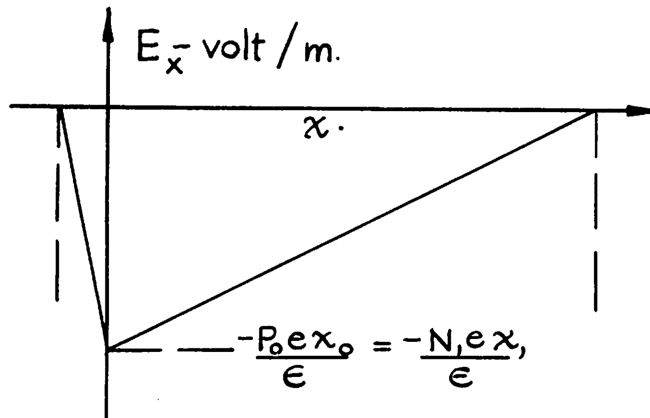

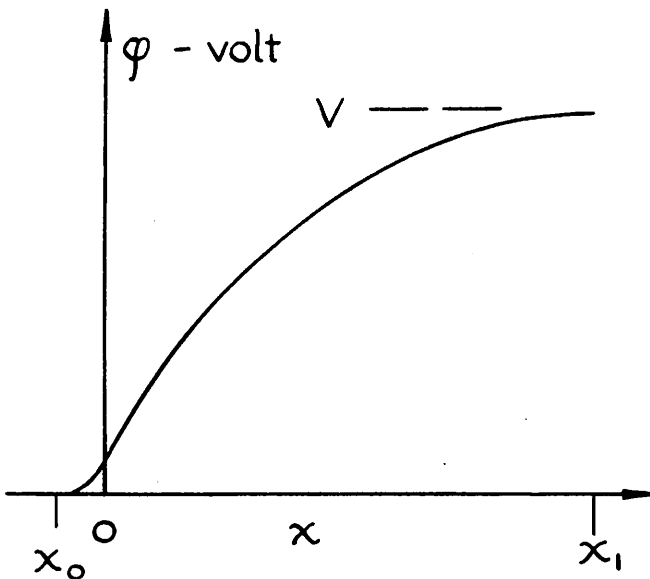

$$\nabla \cdot \vec{E} = \frac{\partial E_x}{\partial x} = \frac{\rho}{\epsilon}$$

<u>case 1</u>. $x \leq 0$

$$\rho = P_o e < 0$$

$$E_{x_o} = \frac{P_o e}{\epsilon}(x - x_o) \leq 0$$

if $\varphi = 0$ @ $x = x_o$

$$\varphi_o = -\frac{P_o e}{2\epsilon}(x - x_o)^2 \geq 0$$

<u>case 2</u>. $x \geq 0$

$$\rho = N_1 e > 0$$

$$E_{x_1} = \frac{N_1 e}{\epsilon}(x - x_1) \leq 0$$

if $\varphi = V$ @ $x = x_1$

$$\varphi_1 = V - \frac{N_1 e}{2\epsilon}(x - x_1)^2 > 0$$

@ $x = 0$ – $E_{x_1} = E_{x_o}$

$$\therefore \; N_1 x_1 = P_o x_o$$

@ $x = 0$ – $\varphi_o = \varphi_1$

$$\therefore V = \frac{e}{2\epsilon}\left(N_1 x_1^2 - P_o x_o^2\right)$$

e = 1.6×10^{-19} coul.
ϵ = dielectric const. - farad/m
P_o = Number of acceptors/m^3
N_1 = Number of donors/m^3

FIG. <u>9.1.</u> VARIATION OF SPACE - CHARGE DENSITY, ELECTRIC FIELD, AND POTENTIAL ACROSS A P - N JUNCTION

9.2. An Indium-Germanium Alloy Junction Diode.

An indium-germanium alloy junction diode made by a carefully controlled process at the Post Office Research Station illustrates the potentialities of the scanning electron microscope for semiconductor surface studies. The model of Fig. 9.1. is well suited to this junction diode, which has a measured donor density N_1 of about 5×10^{14} atoms/cc and an acceptor density P_o estimated at 10^{19} atoms/cc. When a reverse bias of V volts is applied across the junction, the width w of the space-charge region is found from the equations of Fig. 9.1. to be

$$W = \left\{ \frac{2 \epsilon V}{N_1 e} \right\}^{\frac{1}{2}} \approx 2 V^{\frac{1}{2}} \text{ microns,} \qquad (1)$$

where the dielectric constant ϵ of germanium is taken as $16 \epsilon_o$.

Two sets of comparison micrographs with and without reverse bias are shown in Figs. 9.2. and 9.3. Unlike most junctions which have been examined, this junction is seen to be remarkably straight both at low and high magnifications. It was made by alloying an indium pellet onto a single crystal of germanium which had been ground, lapped, and etched to a mirror flat surface along the (111) plane ($\pm$ 30 minutes of arc). By carefully controlling the time-temperature cycle, the indium atoms migrate a constant distance into the germanium, and the alloy junction actually follows a (111) plane over most of its

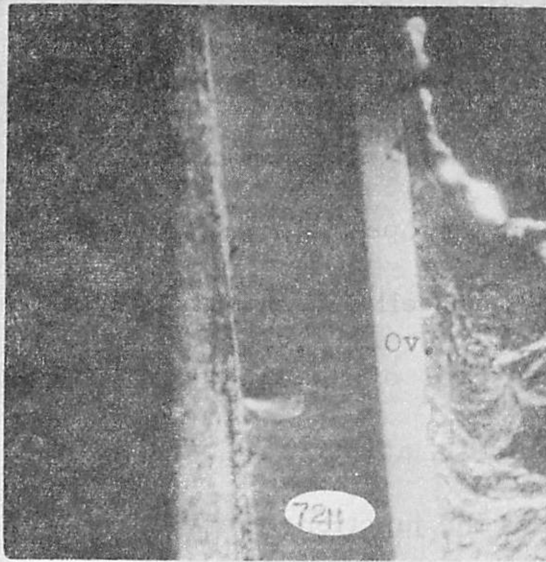

9.2a. Reverse bias = 6 v.

9.2b. No reverse bias.

Fig. 9.2. Comparison micrographs of germanium-indium p-n junction. M = 180.

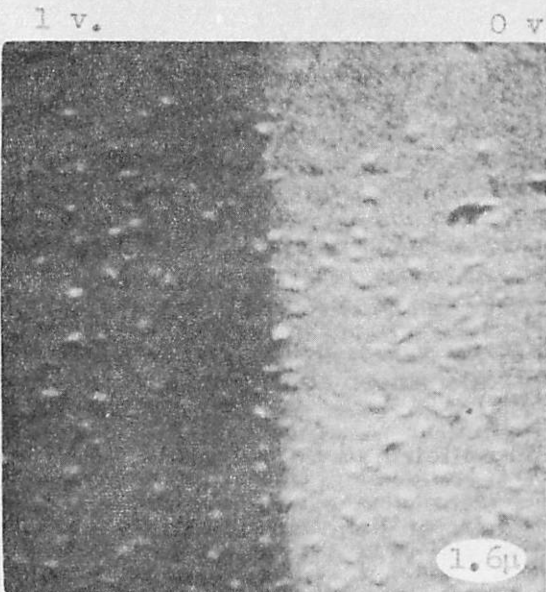

9.3a. Reverse bias = 1 v.

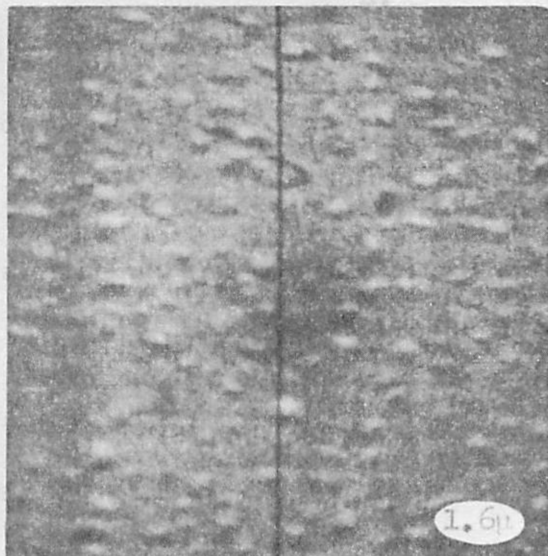

9.3b. No reverse bias.

Fig. 9.3. Higher magnification micrographs of regions on germanium-indium p-n junction. M = 8000.

length, to the resolution of the scanning microscope. Note that a reverse bias of only one volt produces a large contrast in Fig. 9. 3a. (The black line down the centre of Fig. 9. 3b. shows the shutter was inadvertently closed for a few recording scans.)

Other micrographs of special interest are shown in Figs. 9. 4. and 9. 5. Fig. 9. 4a. shows the centre region of the junction is very straight. Fig. 9. 4b. shows the (111) plane which the junction is following changes near the edge of the linear region (this kink is seen most clearly when the micrograph is viewed from a low angle of incidence). The cracks and holes which appear near the bottom of the micrograph are probably the result of crystallographic strain. The region where the junction departs from the (111) plane to curve back to the edge of the germanium crystal is also clearly shown in this micrograph. The shaded area about three microns wide which appears immediately to the left of the junction is believed to represent the space-charge region. The width calculated from (1) agrees well with the observed width on the micrograph. The mechanism of contrast formation in this case may be either transverse fields, as discussed in Chapter 7, or a reduced secondary emission from the space-charge region, where no electrons are present in the conduction band. The comparison micrographs in Fig. 9. 5. show the microscopic roughness of the junction when it can no longer follow a preferred plane, and also illustrate the increased contrast obtained with larger values of reverse bias.

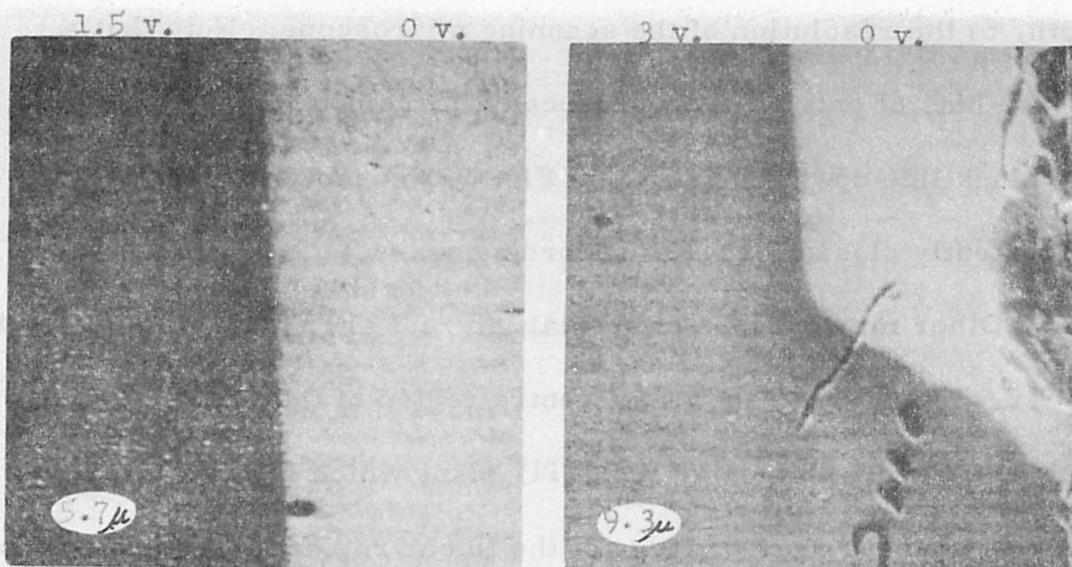

9.4a. Reverse bias = 1.5 v.
M = 2300.

9.4b. Reverse bias = 3 v.
M = 1400.

Fig. 9.4. Regions on germanium-indium junction diode discussed in the text.

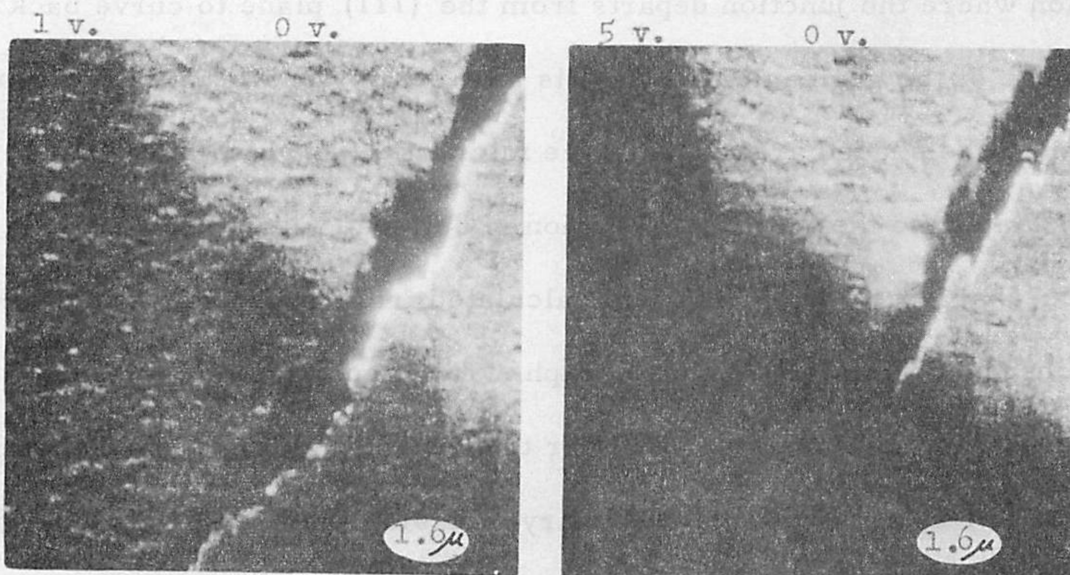

9.5a. Reverse bias = 1 v.

.5b. Reverse bias = 5 v.

Fig. 9.5. Higher magnification micrographs of the centre area of Fig. 9.4b. at different reverse bias voltages.
M = 8300.

9.2.1. Primary Beam-Induced Increase of Reverse-Bias Current.

While recording the above micrographs, an increase in reverse-bias current was observed as the 3 minute recording scan swept over the junction. The following properties of this primary beam-induced reverse-bias current have been observed.

(1) The reverse-bias current through the junction was measured with the 2 frame per second visual scan raster centred on the junction. When the primary beam current was suddenly turned off, the reverse-bias current decreased to a lower value; the decay time was approximately 10 seconds.

(2) The above experiment was repeated using different values of reverse bias. While the results were not completely reproducible, the following trends were apparent. (a) The reverse-bias current induced by the primary beam decreased slowly as a function of time, possibly because of specimen heating or contamination. (b) The ratio of the primary beam-induced reverse-bias current to the beam-off reverse-bias current decreased as the reverse bias increased.

(3) Next the reverse-bias current variation was displayed on an oscilloscope. When the micrograph in Fig. 9.6a. was recorded, the unusually large current variation in Fig. 9.6b. was observed. The form of this current increase is discussed in the next section.

(4) To facilitate the interpretation of subsequent traces, the video signal amplitude was recorded simultaneously with the current

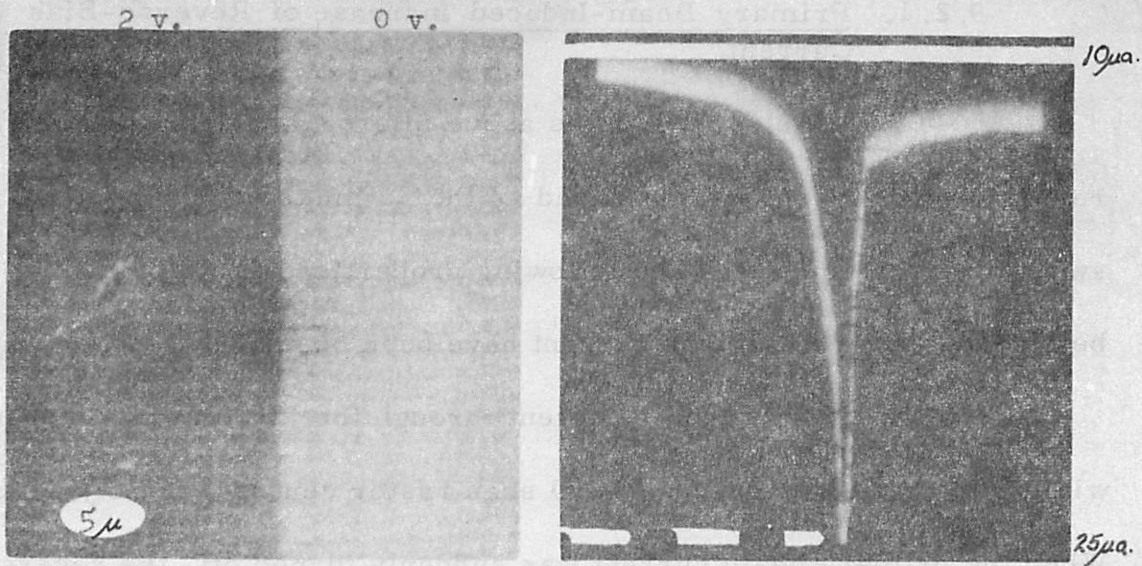

9.6a. Reverse bias = 2 v.
M = 2600

9.6b. Variation of reverse-bias current with primary beam position as 9.6a. was recorded.

Fig. 9.6. Micrograph of p-n junction with CRT trace showing the reverse-bias current increase as the primary beam sweeps over the junction.

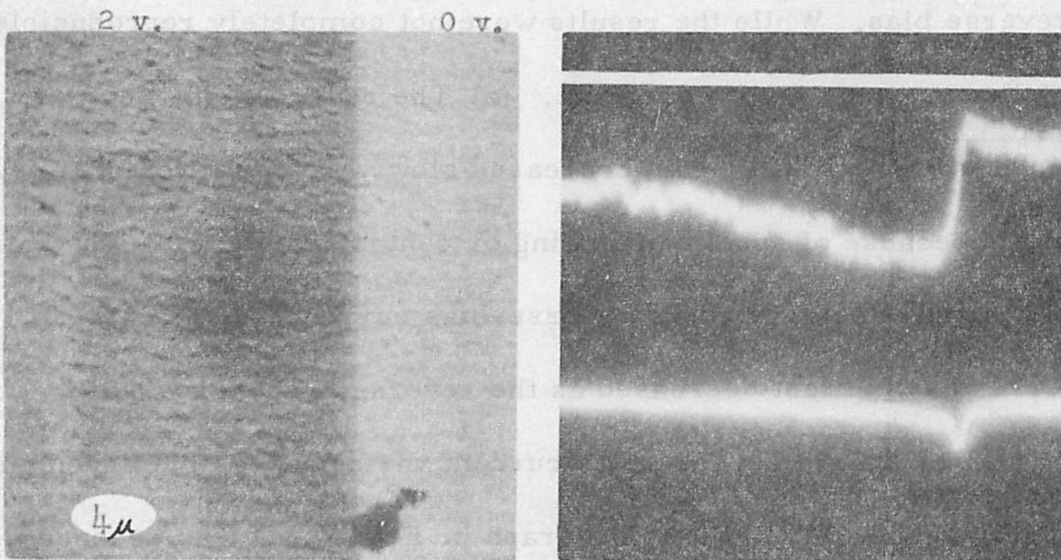

9.7a. Reverse bias = 2v.
M = 3300

9.7b. Top trace: mean video signal.
Bottom trace: reverse-bias current variation.

Fig. 9.7. Micrograph of p-n junction, and CRT traces of mean video signal and reverse-bias current variation.

variation by using the other beam of the oscilloscope. The average brightness variation across the micrograph in Fig. 9.7a. should correspond directly to the top waveform of Fig. 9.7b., which is the mean video signal amplitude. The reverse-bias current variation is shown on the lower trace, and although the peak amplitude is much smaller than that recorded in Fig. 9.6b., the form of the traces appears similar. Note the area of contamination in the centre of Fig. 9.7a.

(5) No increase in current through the junction was observed when low values of forward bias were applied.

(6) The largest increases in current through the junction were measured when either a scratch or a hole was observed at the junction (see Figs. 9.6a. and 9.7a., for example). The increase in reverse-bias current varied considerably with the position of the scanned area along the junction. No increase was detected in certain areas, and large increases, such as recorded in Fig. 9.6b., were observed in only one or two areas.

(7) The form of the reverse-bias current variation vs. primary beam position across the junction seems relatively consistent; the current increases sharply as the primary beam reaches the junction from the P side, and decreases more slowly as the beam proceeds into the N region. Since the recording scan rate is only 2 lines per second (lines parallel to the junction), only very slow decay times

could affect the resulting waveform. Before the scanning coil connections could be reversed to check this point, the EHT set broke down. When the microscope was again in running order several months later, the specimen was so badly deteriorated that further measurements were impossible. Attempts to obtain other carefully processed and sectioned specimens have proved unsuccessful, and the results presented in this section must be regarded as preliminary.

9.2.2. Discussion of the Primary Beam-Induced Increase of Reverse-Bias Current.

Semiconductor surfaces are very complicated compared to the bulk material, and at the present time, are imperfectly understood. Bardeen (1947) initially proposed that surface states exist between the valance and conduction bands, a region forbidden to electrons in the bulk material. More recently surface states with fast (less than 1 microsecond) and slow (1 millisecond to several minutes) minority carrier capture times have been identified (see Kingston, 1956). The density of these states depends upon initial surface treatment, the character of the oxide layer, and the ambient atmosphere to which the surface is exposed. Baker and Yemm (1957) have shown that the depth of surface damage caused by lapping germanium monocrystals similar to the specimen considered above extends 40 to 60 microns into the crystal, and the diffusion distance of minority carriers is greatly reduced in the damaged region.

The energetic electrons injected into the specimen by the primary beam disturb the thermal and electrical equilibrium. They may lose energy in several ways, by creating hole-electron pairs, by exciting electrons and holes from their surface states, and by thermal dissipation, for example. Their charge density will add to, or subtract from the space-charge density near the junction shown in Fig. 9.1.

If the incident beam is 100% efficient in creating hole-electron pairs, when the primary beam energy is 15 kev. and the energy gap of bulk germanium (Kittel, 1953, p.276) is taken as 0.7 volts, the calculated current multiplication is about 4×10^4. For a primary beam current of 25 $\mu\mu$ amp, the resulting increase in current across the junction is about 1 μ amp. Since electron-hole creation by the beam will not be 100% efficient, this is a maximum value. However, in strained areas the energy gap between valance and conduction bands may be less than 0.7 volts, increasing hole-electron pair production. The presence of surface states near the conduction band might also yield a higher carrier production, and the slow decay time mentioned in section 9.2.1., paragraph (1), suggests that surface states play a part in the observed current flow. Thermal effects can be neglected, for the power dissipated in the specimen is less than a microwatt, and the calculated temperature rise is negligible.

As the primary beam scans over the specimen, a very large number of electrons are injected into a very small volume. The range

of 15 kv. electrons in germanium is about 1 micron (from the Thomson-Whiddington Law, with Terrill's constant). If the injected charge is assumed confined to a half-cylinder of radius 1 micron, and of length equal to the length of scan upon the specimen, the average charge density in this volume at a magnification of 3,000 times (a value compatible with Figs. 9.6. and 9.7.) is computed to be 0.15 coulomb/cc. When this charge density, between three and four orders of magnitude greater than the donor density in the N region, is injected into the swept-out area of the N region, it will attract holes from the P region across the junction. However, unless it is captured (by surface states, for example), the increase in current crossing the junction could hardly be more than the primary beam current, some five orders of magnitude less than the observed increase.

The reverse-bias current variations with primary beam position shown in Figs. 9.6b. and 9.7b. are similar to the electric field variation across the junction (shown in Fig. 9.1.). The current increase begins a short distance before the video signal decrease associated with the junction, and does not return to its initial value until after the video signal has assumed a relatively constant value. This behaviour probably indicates that diffusion processes cannot be entirely neglected.

While no firm conclusions about the mechanism of reverse-bias current increase can be drawn from these considerations, it is believed

that given a number of carefully controlled p-n junctions, and the facilities to properly prepare these specimens for microscopic examination, a study of this phenomena would yield a better understanding of semiconductor surfaces. By investigating p-n-p and n-p-n junctions, and using the primary beam to inject electrons into the specimen, phenomena such as avalanche effect could also be studied in a unique way. By observing the variation of reverse-bias current at different primary beam scanning rates, the contributions of slow and fast surface states could be studied. Many other lines of investigation will probably become obvious as the results of initial experiments are evaluated. It should be stressed, however, that such an investigation would require a good supply of suitable semiconductor specimens, proper specimen-preparation facilities, and a reliable scanning microscope.

9.3. Potential Boundaries on a Gallium Phosphide Specimen.

The montage in Fig. 9.8. shows the potential boundaries on a polycrystalline specimen of gallium phosphide (GaP). Striking electroluminescence patterns have been observed on this specimen by Alfrey and Wiggins of the Electron Physics Department, Birmingham University; these patterns seem to occur along grain boundaries, and are believed due to radiative minority carrier recombination occurring at p-n-p junctions, which were formed by impurity segregation at the grain boundaries when the specimen was cooled from the melt (see

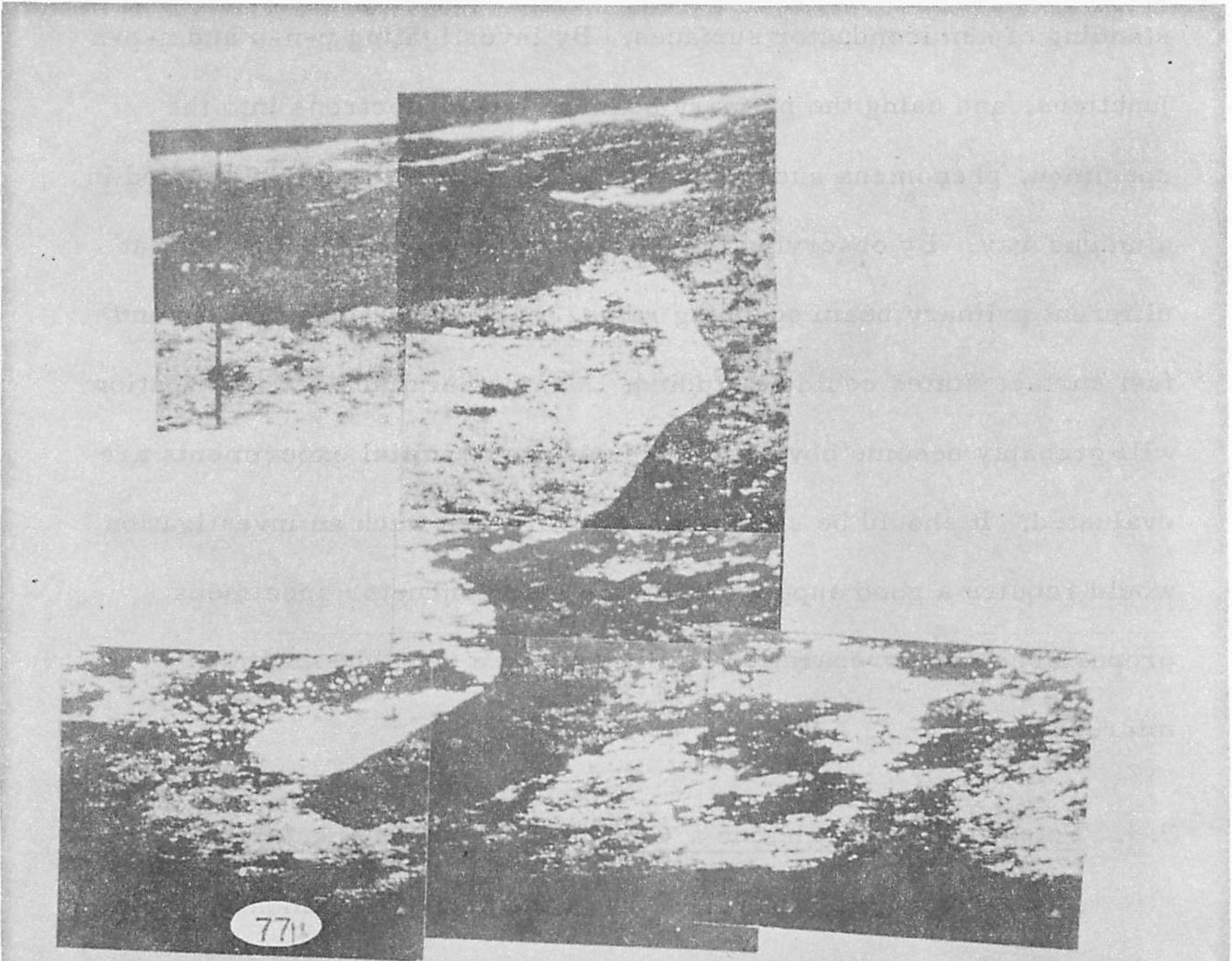

MONTAGE SHOWING POTENTIAL BOUNDARY
ON GALLIUM PHOSPHIDE CRYSTAL SURFACE
6 VOLT BIAS ACROSS CRYSTAL M = 1 100

Fig. 9.8.

Holt, Alfrey, and Wiggins, 1958, and Wiggins, 1957). As mechanical probing proved too coarse to accurately show the potential distribution on the specimen's surface, the scanning microscope was used.

The specimen was provided already mounted for observation as shown in Fig. 9.9. The one-eighth inch diameter specimen stub and the GaP crystal with its leads are embedded in a block of sealing wax; Aquadag painted on the sealing wax around the crystal to prevent charging is also visible. The leads did not make ohmic contact with the crystal, and all bias voltages refer to the drop across both crystal and leads. After the montage shown in Fig. 9.8. was recorded, one lead became disconnected. After it was replaced the three micrographs shown in Fig. 9.10. were recorded with no bias and $\pm$ 7 volts bias respectively. Only specimen contrast appears on the no-bias micrograph, and the potential contrast on the other two micrographs is striking in comparison. At least five different potential regions are visible in Fig. 9.10c., and from the differences between 9.10b. and c, the junctions are clearly not symmetrical over the entire area.

Two montages shown facing each other in Fig. 9.11a. and b show the symmetrical nature of the junction over most of its length. Note that the potential boundary at the top of these montages does not correspond to the potential boundary observed in the earlier montage (Fig. 9.8.). The only change in the specimen which occurred between these examinations was the lead disconnection and replacement

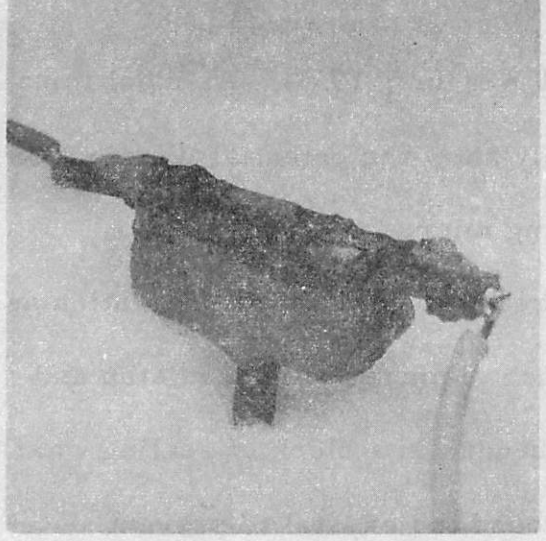

Fig. 9.9. Gallium Phosphide Crystal mounted for examination in the scanning electron microscope.

9.10a. Surface of gallium phosphide crystal, M = 170, no bias.

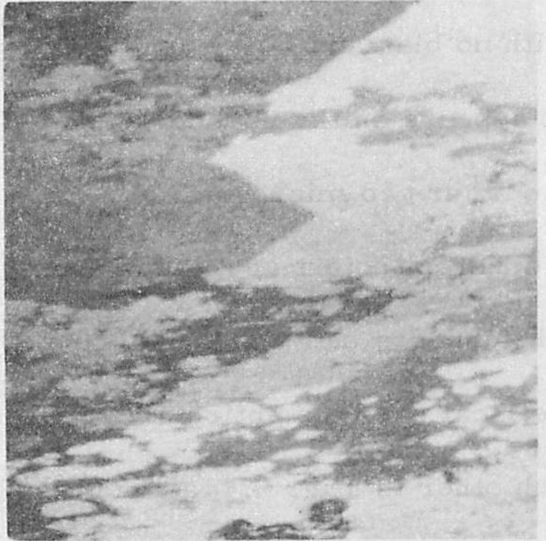

9.10b. Same area, Bias = 7 volts.

9.10c. As 9.9b. with 7 volt bias reversed.

Fig. 9.10. Comparison micrographs of gallium phosphide with no bias and ± 7 volts bias.

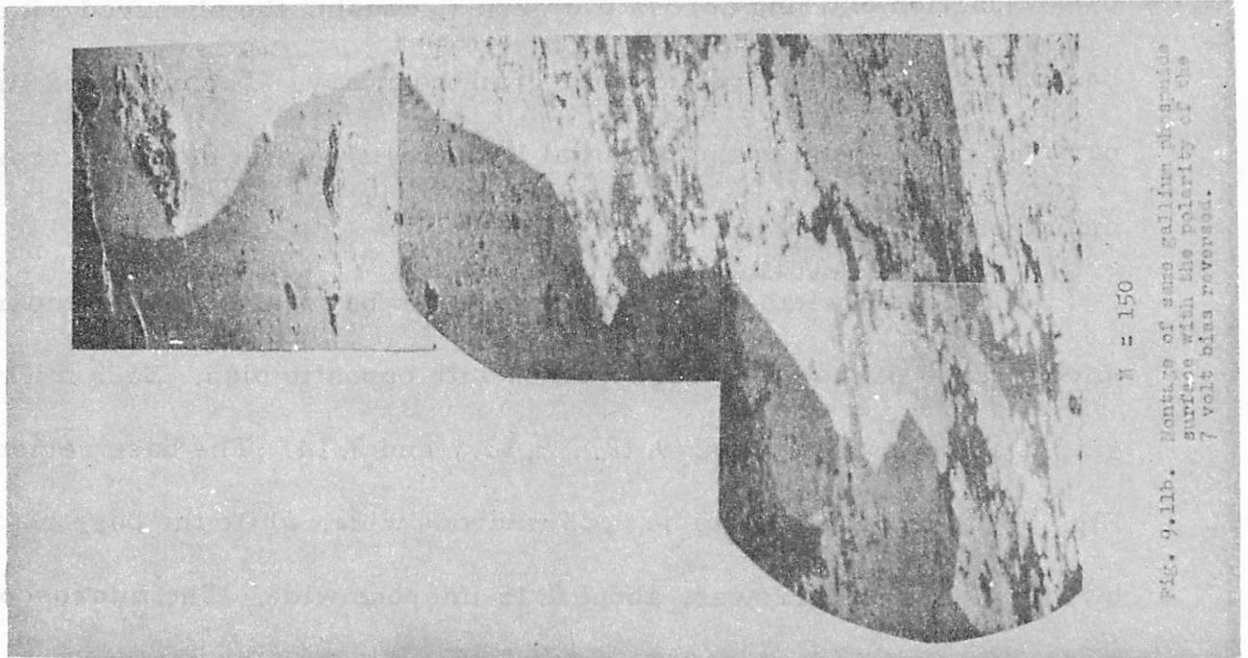

Fig. 9.11b. Montage of same gallium phosphide surface with the polarity of the 7 volt bias reversed. M = 150

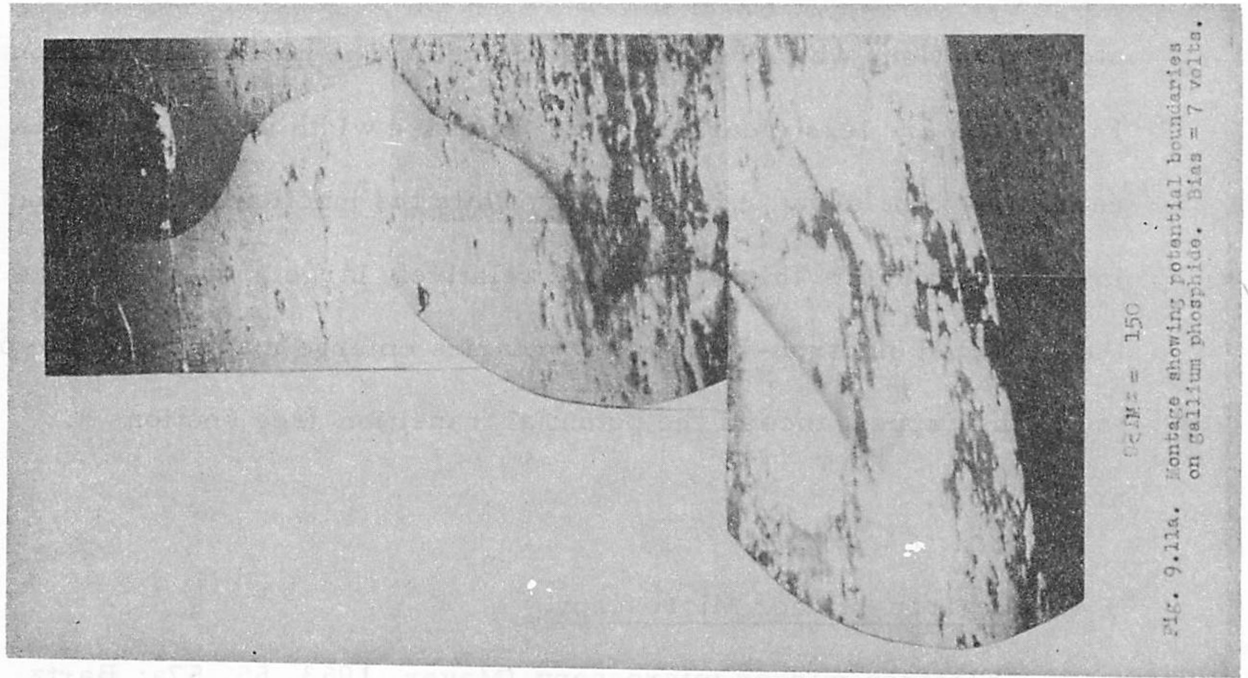

Fig. 9.11a. Montage showing potential boundaries on gallium phosphide. Bias = 7 volts. M = 150

mentioned above. It is possible that the new contact short-circuited the p-n-p junction existing across two grains, causing the observed potential boundary to appear across another grain boundary. The observed light patterns correspond to the potential boundary shown in the more recent montages in Fig. 9.11.

The base width of p-n-p junctions can be measured by comparing micrographs of the same region taken with opposite bias. Such micrographs are shown in Figs. 9.12., 9.13., and 9.14. The base region in Fig. 9.12. is estimated to be 0.25 microns wide, while the base region in Fig. 9.13. is narrower, about 0.15 microns wide. The microscopic roughness of the specimen is apparent in these micrographs, and the etch pits observed along the boundary in Fig. 9.13. are typical of many etched junctions which have been examined. The horizontal junction of Fig. 9.14. are less clearly defined; the base width in this region is estimated to be about 0.5 microns. While the junction itself may be inherently rough in this region, the relatively large area from which the reflected electron-induced secondaries emerge may contribute to the diffuse appearance of the potential transition (see sections 4.2. and 5.6.2.).

9.4. Electron Mirror Microscopy.

Electron mirror microscopy (Mayer, 1953, 55, 57a; Bartz, Weissenberg, and Wiskott, 1956; and Wiskott, 1956, 56a) is another electron-optical method of imaging potential differences on a specimen

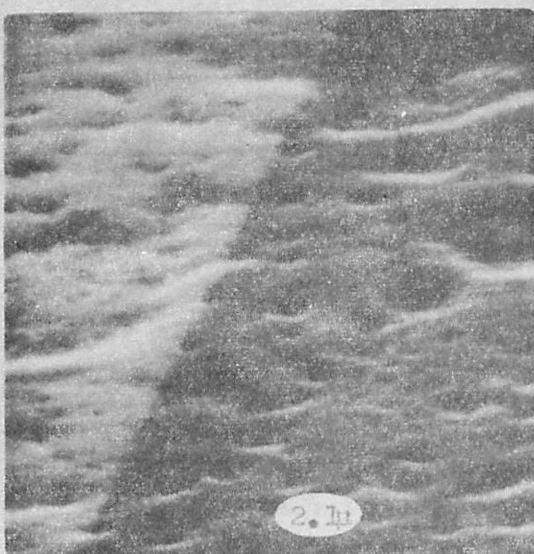

9.12a. M = 6200,
Bias = 10 v.

9.12b. Same as 9.12a. except
10 v. bias reversed.

Fig. 9.12. Higher magnification micrographs of gallium phosphide showing width of base region in p-n-p junction.

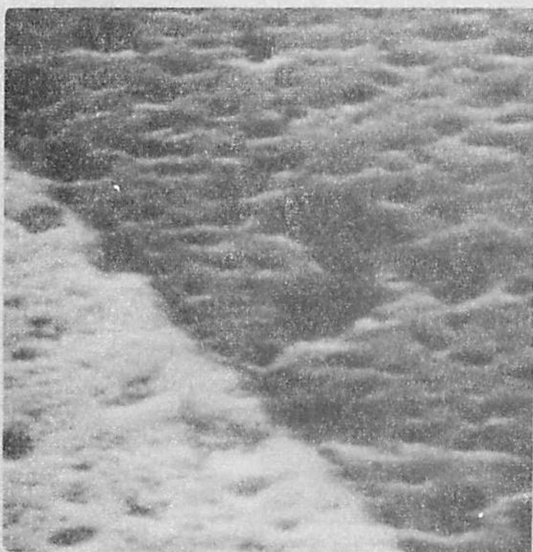

9.13a. M = 5800,
Bias = 10 v.

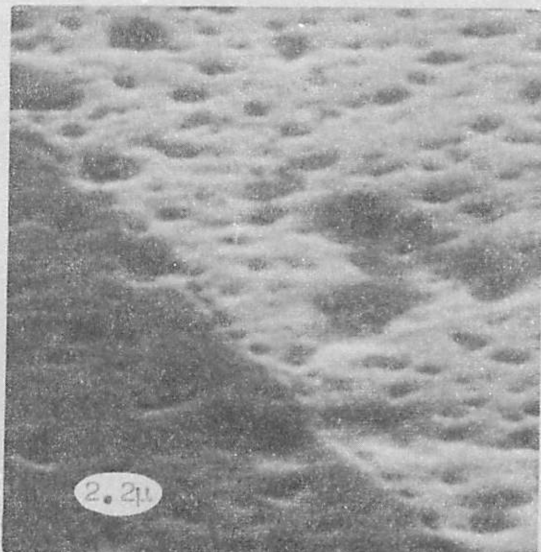

9.13b. Same as 9.13a. except
10 v. bias reversed.

Fig. 9.13. As Fig. 9.12., at a different position on the junction.

9.14a. M = 6400, bias = 10 v.

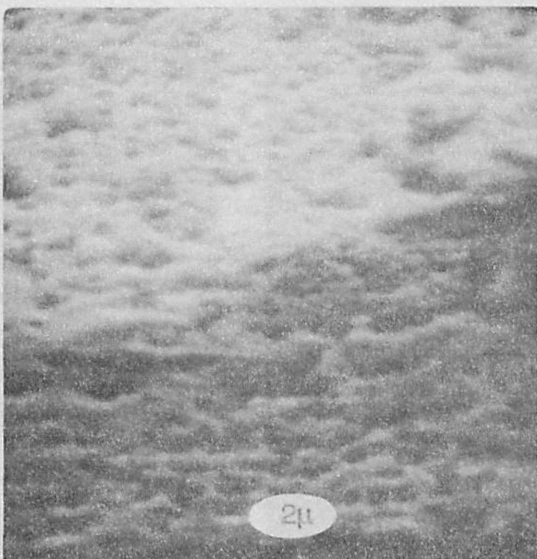

9.14b. M = 6400, 10 v. bias reversed.

Fig. 9.14. As Fig. 9.12., at a different position on the junction. Bias = ± 10 v.

surface. The specimen is normally held slightly below cathode potential, and acts as a mirror to the electrons directed toward it. The electrons are reflected at equipotential surfaces very near the specimen, and any geometrical variation in these equipotential surfaces caused by either potential differences or geometrical relief on the specimen surface produces contrast on the image. Magnetic fields above the specimen surface will also deflect the electrons, and thus produce contrast on the image (Mayer, 1957b, 1958).

The mean electric field toward the specimen ranges from 1 to 100 kv/cm, and attracts positive ions produced by the electron beam to the specimen. Electrons emitted from a thermionic cathode have a Maxwellian distribution, and the high-energy electrons in the tail of this distribution strike the specimen also. The maximum resolution of this instrument has been estimated by Wiskott (1956b, p. 493) to be about 150 A. with 100 kv/cm field at the specimen. Mayer (1955, p. 1229) has reported an experimental value of 3000 A., and has implied in a more recent paper (Mayer, 1957, p. 975) that a resolution of 600 A. has been obtained. He has stressed that electron mirror micrographs require careful interpretation because the potential relief in front of the specimen, not the specimen itself, is imaged. Also, the high value of electric field at the specimen is a disadvantage in certain applications, and the specimen itself must be relatively smooth both geometrically and electrically for reasonable results.

In scanning electron microscopy, interpretation is easy because object and image picture elements correspond directly. There is only a low electric field at the specimen (and this could be eliminated if necessary), and rough specimens, the bane of most other electron-optical devices, are imaged with ease. Thus electron mirror microscopy complements, rather than rivals, scanning electron microscopy.

REFERENCES

BAKER, D., and YEMM, H., Brit. J. Appl. Phys. 8, 302, (1957).

BARDEEN, J., Phys. Rev. 71, 717, (1947).

BARTZ, G., WEISSENBERG, G., and WISKOTT, D., Proc. Int. Conf. Electron Microscopy, London, 1954, p. 395, (1956).

BECKER, A., Ann. Physik 2, 249, (1929).

BIRKHOFF, R. D., Handbuch der Physik, XXXIV, 53, (Springer - Verlag, Berlin, 1958).

BIRKS, J. B., Scintillation Counters, (Pergamon Press Ltd., London, 1953).

BITTER, F., Phys. Rev. 38, 1903, (1931).

BLACKMAN, M., and GRÜNBAUM, E., Nature 178, 584, (1956).

BOTHE, W., Z. Naturforsch. 4a, 542, (1949a).

BOTHE, W., Ann. Physik 6, 44, (1949b).

BRICKA, M., and BRUCK, N., Ann. Radioelectricite, 3, 339, (1948).

BRUINING, H., Physics and Application of Secondary Electron Emission, (Pergamon Press Ltd., London, 1954).

COPELAND, P. L., Phys. Rev. 58, 604, (1940).

COSSLETT, V. E., Practical Electron Microscopy, (Butterworths Scientific Publications, London, 1951).

COSSLETT, V. E., and HAINE, M. E., Proc Int. Conf. Electron Microscopy, London, 1954, p. 639, (1956).

DEKKER, A. J., Solid State Physics, (Prentice-Hall, Inc., Englewood Cliffs, New Jersey, 1957).

DUNCUMB, P., Microanalysis with an X-ray Scanning Microscope, (Ph. D. Thesis, University of Cambridge, 1957).

DUNLAP, W. C., An Introduction to Semiconductors, (John Wiley and Sons, Inc., New York, 1957).

DYKE, W. P., and DOLAN, W. W., Advances in Electronics and Electron Physics VIII, 90, (Academic Press, Inc., New York, 1956).

GOLDSTEIN, H., Classical Mechanics, (Addison-Wesley Press, Inc., Cambridge, Mass., 1951).

HAINE, M. E., and EINSTEIN, P. A., Brit. J. Appl. Phys. 3, 40, (1952).

HALL, C. E., Introduction to Electron Microscopy, (McGraw-Hill Book Company, Inc., New York, 1953).

HARDY, A. C. and PERRIN, F. H., The Principles of Optics, (McGraw-Hill Book Company, Inc., New York, 1932).

HENNEY, K., and DUDLEY, B., Handbook of Photography, (McGraw-Hill Book Company, Inc., New York, 1939).

HERRMANN, G., and WAGENER, S., The Oxide-Coated Cathode, Vol. II, (Chapman and Hall Ltd., London, 1951).

HIBI, T., J. Electron Microscopy 4, 10, (1956).

HOLLAND, L., Vacuum Deposition of Thin Films, (Chapman and Hall, London, 1956).

HOLLIDAY, J. E., and STERNGLASS, E. J., J. Appl. Phys. 28 1189, (1957).

HOLT, D. A., ALFREY, G. F., and WIGGINS, C. S., Nature 181 109, (1958).

HOPKINSON, R. G., Jour. IEE 93, Part 3A, 808, (1946).

JONKER, J. L. H., Philips Res. Rep. 6, 372, (1951).

JONKER, J. L. H., Philips Res. Rep. 7, 1, (1952).

TERRILL, H. M., Phys. Rev. 22, 101, (1923).

THOMSON, J. J., Conduction of Electricity Through Gases, 2nd Edition, (Cambridge University Press, Cambridge, 1906).

VALLEY, G. E., and WALLMAN, H., Vacuum Tube Amplifiers, (McGraw-Hill Book Company, Inc., New York, 1948).

van der ZIEL, A., Noise, (Chapman and Hall, Ltd., London, 1955).

von ARDENNE, M., Z. Phys. 109, 553, (1938).

WELLS, O. C., The Construction of a Scanning Electron Microscope and its Application to the Study of Fibres, (Ph. D. Thesis, University of Cambridge, 1957).

WHIDDINGTON, R., Proc. Roy. Soc. 89A, 554, (1914).

WIGGINS, C. S., Electroluminescence in Gallium Phosphide, (M. Sc. Thesis, University of Birmingham, 1957).

WISKOTT, D., Optik 13, 463, (1956a).

WISKOTT, D., Optik 13, 481, (1956b).

WRIGHT, W. D., The Perception of Light, (Blackie and Son, Ltd., London, 1938).

YOUNG, J. R., J. Appl. Phys. 28, 524, (1957).

ZWORYKIN, V. K., HILLIER, J., and SNYDER, R. L., A.S.T.M. Bull. 117, 15, (August 1942).

ZWORYKIN, V. K., MORTON, G. A., RAMBERG, E. G., HILLIER, J., and VANCE, A. W., Electron Optics and the Electron Microscope, (John Wiley and Sons, Inc., New York, 1945).

ZWORYKIN, V. K., and MORTON, G. A., Television, (John Wiley and Sons, Inc., New York, 1954).

HANDBOOK OF CHEMISTRY AND PHYSICS, (Chemical Rubber Publishing Company, Cleveland, 1949).

McMULLAN, D., Investigations Relating to the Design of Electron Microscopes, (Ph. D. Thesis, University of Cambridge, 1952).

McMULLAN, D., Proc. IEE 100, Pt. 2, 245, (1953).

MÜLLER, H. O., Z. Phys. 104, 475, (1937).

MYTUM, E., Photography 8, 55, (1958).

NELMS, A., Nat. Bur. Standards Circ. 577, 1-30, (1956).

OATLEY, C. W., and EVERHART, T. E., J. Electronics 2, 568, (1957).

PAGE, D. H., Brit. J. Appl. Phys. 9, 60, (1958).

PALLUEL, P. C. R., C. R. Acad. Sci. Paris 224, 1492 and 1551, (1947).

PIERCE, J. R., Theory and Design of Electron Beams, (D. Van Nostrand Company, Inc., New York, 1954).

PIZER, H. I., YATES, J. G., and SANDER, K. F., J. Electronics 2, 65, (1956).

REGENSTREIF, E., Théorie de la Lentille Électrostatique a Trois Électrodes, (Ph. D. Thesis, University of Paris, 1951).

ROSE, A., Advances in Electronics I, 131, (Academic Press, Inc., New York, 1948).

SHOCKLEY, W., and PIERCE, J. R., Proc. IRE 26, 321, (1938).

SMITH, K. C. A., The Scanning Electron Microscope and its Fields of Application, (Ph. D. Thesis, University of Cambridge, 1956).

SMITH, K. C. A., and OATLEY, C. W., Brit. J. Appl. Phys. 6, 391, (1955).

STERNGLASS, E. J., Phys. Rev. 95, 345, (1954).

STERNGLASS, E. J., and WACHTEL, M. M., Phys. Rev. 99, 646A, (1955).

JONKER, J. L. H., Philips Res. Rep. 9, 391, (1954).

JONKER, J. L. H., Philips Res. Rep. 12, 249, (1957).

KANTER, H., Ann. Physik 20, 144, (1957).

KATZ, L., and PENFOLD, A. S., Rev. Mod. Phys. 24, 28, (1952).

KINGSTON, R. H., J. Appl. Phys. 27, 101, (1956).

KITTEL, C., Introduction to Solid State Physics, (John Wiley and Sons, Inc., New York, 1953).

KURRELMEYER, B., and HAYNER, L. J., Phys. Rev. 52, 952, (1937).

LANE, R. O., and ZAFFARANO, D. J., Phys. Rev. 94, 960, (1954).

LANGMUIR, D. B., Proc. IRE 25, 977, (1937).

LAX, L., and WEIGHTON, D., Proc. IEE 99, Pt. 3A, 804, (1952).

MARCH, A. A. C., A Scanning Microdensitometer and Bismuth Oxide Films, (Ph. D. Thesis, University of Cambridge, 1957).

MARTON, L., Nat. Bur. Standards Circ. 527, Electron Physics, p. 1, (1954).

MASSEY, H. S. W. and BURHOP, E. H. S., Electronic and Ionic Impact Phenomena, (Oxford University Press, London, 1952).

MAYER, L., J. Appl. Phys. 24, 105, (1953).

MAYER, L., J. Appl. Phys. 26, 1228, (1955).

MAYER, L., J. Appl. Phys. 28, 259, (1957a).

MAYER, L., J. Appl. Phys. 28, 975, (1957b).

MAYER, L., J. Appl. Phys. 29, 658, (1958).

McKAY, K. G., Advances in Electronics I, 66, (Academic Press, Inc., New York, 1948).